NASA TECHNICAL NOTE

NASA TN D-8104

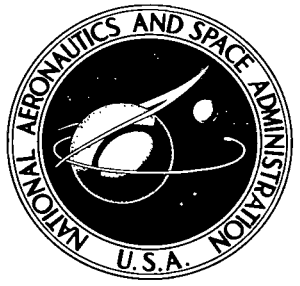

NASA TN D-8104

EVIDENCE OF THE BEAM PATTERN CONCEPT OF SUBSONIC JET NOISE EMISSION

S. Paul Pao and Lucio Maestrello

Langley Research Center
Hampton, Va. 23665

NATIONAL AERONAUTICS AND SPACE ADMINISTRATION • WASHINGTON, D. C. • FEBRUARY 1976

1. Report No. NASA TN D-8104	2. Government Accession No.	3. Recipient's Catalog No.
4. Title and Subtitle EVIDENCE OF THE BEAM PATTERN CONCEPT OF SUBSONIC JET NOISE EMISSION		5. Report Date February 1976 6. Performing Organization Code
7. Author(s) S. Paul Pao and Lucio Maestrello		8. Performing Organization Report No. L-10479
9. Performing Organization Name and Address NASA Langley Research Center Hampton, Va. 23665		10. Work Unit No. 505-03-11-02 11. Contract or Grant No.
12. Sponsoring Agency Name and Address National Aeronautics and Space Administration Washington, D.C. 20546		13. Type of Report and Period Covered Technical Note 14. Sponsoring Agency Code
15. Supplementary Notes		

16 Abstract

This study describes the methods and results of a new approach toward positively identifying the apparent location and strength of the sound source in a subsonic jet. The Green's function technique is applied to regenerate the three-dimensional distribution of the acoustic far field from measured data on a two-dimensional plane. The apparent sound-source location is also determined by using geometrical ray acoustics. The results revealed a number of features of the subsonic jet noise mechanisms. They show that the apparent sound source is highly localized within the jet flow and that the spontaneous noise emission from such a compact source volume is in the fashion of a narrow beam with random directions. These observable properties of the sound field offer the basis for a beam pattern concept of subsonic jet noise radiation. This study not only provides the immediate benefit of new insight into the mechanisms of subsonic noise radiation but also verifies a powerful and accurate technique of aerodynamic noise measurements. This technique is expected to have important applications in the development of jet noise reduction technology.

17. Key Words (Suggested by Author(s)) Jet noise Subsonic jet	18. Distribution Statement Unclassified – Unlimited Subject Category 71		
19. Security Classif. (of this report) Unclassified	20. Security Classif. (of this page) Unclassified	21. No. of Pages 47	22. Price* $3.75

*For sale by the National Technical Information Service, Springfield, Virginia 22161

EVIDENCE OF THE BEAM PATTERN CONCEPT OF SUBSONIC JET NOISE EMISSION

S. Paul Pao and Lucio Maestrello
Langley Research Center

SUMMARY

This study describes the methods and results of a new approach toward positively identifying the apparent location and strength of the sound source in a subsonic jet. The Green's function technique is applied to regenerate the three-dimensional distribution of the acoustic far field from measured data on a two-dimensional plane. The apparent sound-source location is also determined by using geometrical ray acoustics. The results revealed a number of features of the subsonic jet noise mechanisms. They show that the apparent sound source is highly localized within the jet flow and that the spontaneous noise emission from such a compact source volume is in the fashion of a narrow beam with random directions. These observable properties of the sound field offer the basis for a beam pattern concept of subsonic jet noise radiation. This study not only provides the immediate benefit of new insight into the mechanisms of subsonic noise radiation but also verifies a powerful and accurate technique of aerodynamic noise measurements. This technique is expected to have important applications in the development of jet noise reduction technology.

INTRODUCTION

The continual requirement for advances in jet noise reduction has provided a strong stimulus for research in the area of positive identification of dominant noise production mechanisms within the jet flow. Such work demands a substantial degree of refinement in both the experimental and analytical techniques. Several ways of making measurements to determine the sound-source location have been used: (a) direct measurement of the fluctuating velocity or density within the jet, where the sound-source strength is calculated according to theoretical models; (b) cross correlation between measurements of fluctuating aerodynamic quantities in the jet and the acoustic measurements in the far field, where sound-source strength distribution is determined by analyzing the cross correlation functions; and (c) acoustic measurements near the jet, where either mechanical or analytical acoustic imaging techniques are used to recover the apparent sound-source distribution within the jet. The present study belongs to the third category. It attempts to advance the

state of the art in this area. Some background for this study is found in references 1 and 2.

The acoustic field surrounding a subsonic jet is an intricate distribution of wave vectors. The sound-pressure fluctuation at each point near the jet is a summation of contributions from a large volume of the jet flow. From an experimental point of view, both the amplitude and phase information of the received acoustic signal must be resolved in order to retain sufficient information to detect the location and strength of the apparent sound source in the jet. Mutually independent pointwise measurements commonly chosen for jet noise directivity measurements cannot resolve such details. Some highly successful results in determining apparent sound-source strength distribution are reported in references 3 and 4 where mirror imaging techniques are employed.

Enough data to provide a comprehensive description of the sound field can be obtained through the measurement of the space-time correlation function of the normal sound-pressure gradient over an imaginary plane near the jet. Reference 5 presents data obtained from such a measurement. That study computed the normal acoustic energy flux at the plane of measurement near the jet. Although the space-time correlation data contain all the necessary information to regenerate a detailed description of the sound field surrounding the jet, the original data alone cannot convey an intuitive and direct impression of the sound emission and propagation process. The basic purpose of this study is to retrieve meaningful numerical representations of the sound field surrounding this subsonic jet.

In this study, two methods of data analysis are given. The first method is the direct integration approach using the Green's function technique. This approach is capable of recovering from the data quantities such as the three-dimensional distribution of sound-pressure intensity, the correlation functions of sound pressure in the far field, and the visualization of the motion of a statistical wave front. In the second method, a simple triangulation technique based on geometrical acoustic considerations is developed. This technique is relatively simple although it is capable of providing accurate information about the apparent sound-source location in the jet flow and the far-field sound propagation patterns.

This study, by providing positive information about the subsonic jet noise emission pattern, is intended to contribute to research in the area of jet noise reduction. The methods of analysis, a description of the existing data, discussion of results, and the physical evidences leading to the beaming concept of subsonic jet noise radiation are given in the following sections.

SYMBOLS

c	constant speed of sound
D	diameter of jet
$D[\bar{R}_{pp}]$	differential correlation function
d	distance of separation of two points
f	frequency, Hz
n_0	normal direction with respect to plane of measurement
p	sound pressure
q	equivalent sound-source distribution
R	radial distance
R_{pp}	sound-pressure correlation function
$R_{\gamma\gamma}$	correlation of intermittency factor
$R_{\nabla p \nabla p}$	normal sound-pressure gradient correlation function
r	radius measured from jet axis
r_1	$= \lvert \underset{\sim}{x} - \underset{\sim}{y} \rvert$
r_2	$= \lvert (\underset{\sim}{x} + \underset{\sim}{\xi}) - (\underset{\sim}{y} + \underset{\sim}{\eta}) \rvert$
S	designation of surface in three-dimensional space
S_{pp}	cross spectral density function of sound pressure
S_{qq}	cross spectral density function of apparent sound source
$S_{\nabla p \nabla p}$	cross spectral density function of normal sound-pressure gradient

$S(y), S(\eta)$ range of integration for surface integral

$dS, dS(y), dS(\eta)$ infinitesimal surface element

t time variable

t' retarded time variable

U_j jet exit velocity

$V(y), V(\eta)$ range of integration for volume integral

$\dot{W}$ sound power

W_t total sound power from jet

(X,Y,Z) local Cartesian coordinate system

(X',Y') local two-dimensional coordinate system on plane in far field

$\underset{\sim}{x}$ general three-dimensional variable in free space

x_j distance along axis of jet

$\underset{\sim}{y}$ general two- or three-dimensional variable in source region

$dy^3, d\eta^3$ infinitesimal volume element

Z' average direction of ray bundle

γ intermittency factor

Δ finite differential quantity

δ infinitesimal differential quantity

η spatial separation distance which takes both positive and negative values

$\underset{\sim}{\eta}$ spatial separation vector in source region

θ	angle measured in X,Z-plane as measured from X-axis
ξ	spatial separation distance in far field
$\underset{\sim}{\xi}$	spatial separation vector in far field
ρ_0,ρ_1	differential correlation coefficients
τ,τ^*	delay time variables
τ_{max}	delay time value at which correlation reaches maximum
ϕ	azimuth angle in local spherical coordinate systems
ϕ^*	angular variable around circumference of jet
ψ	angle in local spherical coordinate system
ω	circular frequency

BASIC ANALYSIS

The theory of wave propagation states that if the sound source can be described as a known function of space and time, the induced sound field throughout the free space can be computed. In some cases, however, the sound source is not known although an equivalent mathematical condition can be established. In figure 1, a distributed acoustic source is enclosed by a surface S in a three-dimensional homogeneous medium. If the time-varying normal sound-pressure gradient on this surface S induced by the source distribution inside is known, the induced sound field throughout the free space outside of the surface S can be computed by using the appropriate Green's function. Such an equivalent representation of the sound source is most useful in the case of subsonic jet noise measurement because the strength of the aerodynamic sound sources within the jet is not yet amenable to direct measurements. Instead of direct source measurements, equivalent acoustic measurements can be made on a surface within the acoustic field near the jet. Figure 2 shows the geometrical arrangement of such a measurement which was reported in reference 5. The surface S becomes simply an infinite plane separating the space into two halves: the inner half which contains the subsonic jet exhaust flow and the outer half which is source free. The acoustic data in reference 5 were obtained in the form of space-time correlation functions of the normal sound-pressure gradients on this plane.

The basic aim of this study is to obtain from the data meaningful numerical representations of the sound field surrounding this subsonic jet. Although the space-time correlation functions on the plane contain all the information to regenerate the kinematics of the sound field, the original data alone lack the ability to convey an intuitive and direct image of the sound emission and propagation process; consequently, further analysis is in order. In this section on basic analysis, the key mathematical tools for extracting useful information from the data are discussed.

The Green's Function Formulation

Derivation of the integral formulae.- Analytically, the sound field in the source free half-space can be computed from the prescribed data of a normal sound-pressure gradient on the data plane if the acoustic process under consideration is deterministic. The Green's function of the wave equation satisfying a Neumann boundary condition on the plane is used in the integral formula:

$$\left.\begin{aligned} p(\underset{\sim}{x},t) &= \frac{1}{2\pi}\int_S \frac{1}{|\underset{\sim}{x}-\underset{\sim}{y}|}\left[\frac{\partial p}{\partial n_0}(\underset{\sim}{y},t')\right] dS \\ t' &= t - \frac{|\underset{\sim}{x}-\underset{\sim}{y}|}{c} \end{aligned}\right\} \qquad (1)$$

where p is the sound pressure, c is the speed of sound, $\underset{\sim}{x}$ is a point in the source free half-space, t is the time, dS is an infinitesimal surface element on the data plane, $\underset{\sim}{y}$ is a point on the data plane, n_0 is the normal to the plane, and the bracket around the pressure-gradient function indicates that the function should be evaluated at an appropriate retarded time t'.

In this study, the sound-pressure fluctuations can be considered as a stationary random process. Only the statistical functional values of the sound field can be meaningful. An expression which relates the sound-pressure correlation function to the sound-pressure gradient correlation function can be derived:

$$R_{pp}(\underset{\sim}{x},\underset{\sim}{\xi},\tau) = \frac{1}{4\pi^2}\iint_{S(y),S(\eta)} \frac{R_{\nabla p \nabla p}(\underset{\sim}{y},\underset{\sim}{\eta},\tau^*)}{|\underset{\sim}{x}-\underset{\sim}{y}|\,|\underset{\sim}{x}+\underset{\sim}{\xi}-(\underset{\sim}{y}+\underset{\sim}{\eta})|}\, dS(y)\, dS(\eta) \qquad (2)$$

$$R_{pp}(\underset{\sim}{x},\underset{\sim}{\xi},\tau) = \left\langle p(\underset{\sim}{x},t)\, p(\underset{\sim}{x}+\underset{\sim}{\xi}, t+\tau)\right\rangle$$

$$R_{\nabla p \nabla p}(\underset{\sim}{y},\underset{\sim}{\eta},\tau^*) = \left\langle \frac{\partial p}{\partial n_0}(\underset{\sim}{y},t)\frac{\partial p}{\partial n_0}(\underset{\sim}{y}+\underset{\sim}{\eta}, t+\tau^*)\right\rangle$$

$$\tau^* = \tau - \frac{|\underset{\sim}{x}+\underset{\sim}{\xi}-(\underset{\sim}{y}+\underset{\sim}{\eta})| - |\underset{\sim}{x}-\underset{\sim}{y}|}{c}$$

The value $R_{pp}(\underset{\sim}{x},\underset{\sim}{\xi},\tau)$ is the sound-pressure correlation function as defined in the half-space, $R_{\nabla p \nabla p}(\underset{\sim}{y},\underset{\sim}{\eta},\tau^*)$ is the normal sound-pressure gradient correlation function as defined over the data plane, $\underset{\sim}{x}$ and $\underset{\sim}{y}$ are the reference points for correlation, $\underset{\sim}{\xi}$ and $\underset{\sim}{\eta}$ are the spatial separation vectors, $dS(y)$ and $dS(\eta)$ are the infinitesimal surface elements for integration on the plane corresponding to the $\underset{\sim}{y}$ and the $\underset{\sim}{\eta}$ variables, τ is the delay time, and τ^* is the delay time for the source function where appropriate retarded time relations have been taken into account.

The right-hand side of equation (2) is a double surface integral; each integral has an infinite range of integration over the entire data plane. The $\underset{\sim}{y}$-variable is fixed for the integration with respect to η. Therefore, the source function in this first step of integration is simply a space-time correlation function with respect to a single reference point on the data plane. Such a space-time correlation function is what is commonly measured in an experiment. A physical interpretation of this first integral can be provided. Equation (2) is the statistical average of the joint contribution of $\partial p/\partial n_0$ from an infinitesimal area element at $\underset{\sim}{y}$ and $\partial p/\partial n_0$ from all over the data plane, while the function $R_{\nabla p \nabla p}(\underset{\sim}{y},\underset{\sim}{\eta},\tau^*)$ helps to reduce the range of integration to an effectively finite domain on the data plane. Since all the contributions related to the sound-pressure gradient at $\underset{\sim}{y}$ have been taken into account, this first integral represents the total acoustic contribution from the jet transmitted through an infinitesimal area at $\underset{\sim}{y}$. Hence, the subsequent integration over the $\underset{\sim}{y}$-variable provides the sum of all the contributions from the acoustic source as transmitted through this plane.

In this study, the available data consist of correlation functions measured at a limited number of reference points in the $\underset{\sim}{y}$-variable. Such data can best be used for the study of the local sound emission properties at various parts of the jet flow. Integration over the $\underset{\sim}{y}$-variable is not discussed. Since only one integral in equation (2) is evaluated, the equation can best be written in a differential form:

$$\frac{\delta R_{pp}(\underset{\sim}{x},\underset{\sim}{\xi},\tau)}{\delta S(y)} = \frac{1}{4\pi^2} \int_{S(\eta)} \frac{R_{\nabla p \nabla p}(\underset{\sim}{y},\underset{\sim}{\eta},\tau^*)}{\left|\underset{\sim}{x} - \underset{\sim}{y}\right| \left|\underset{\sim}{x} + \underset{\sim}{\xi} - (\underset{\sim}{y} + \underset{\sim}{\eta})\right|} \, dS(\eta)$$

It is convenient to define

$$D\left[R_{pp}(\underset{\sim}{x},\underset{\sim}{\xi},\tau)\right] \equiv \frac{\delta R_{pp}(\underset{\sim}{x},\underset{\sim}{\xi},\tau)}{\delta S(y)} \tag{3}$$

The quantity $D\left[R_{pp}(\underset{\sim}{x},\underset{\sim}{\xi},\tau)\right]$ is called the differential correlation function and represents the acoustic contribution to the correlation function $R_{pp}(\underset{\sim}{x},\underset{\sim}{\xi},\tau)$ from a unit area in the neighborhood of the fixed point $\underset{\sim}{y}$ on the data plane.

For economy of numerical computation, it is worthwhile to consider the meaning of this function. The function $D\left[R_{pp}(\underset{\sim}{x},\underset{\sim}{\xi},\tau)\right]$ depends on seven independent variables. Consider first the case with $\underset{\sim}{x}$ fixed. The restricted function then depends on four independent space and time variables. In general, this differential correlation function represents the linear dependence between sound-pressure signals at a fixed point and at a variable point for all values of time delay. In essence, such linear dependence can be classified as either time-like or space-like:

(a) The time-like property of sound-pressure correlation between two points $\underset{\sim}{x}$ and $\underset{\sim}{x} + \underset{\sim}{\xi}$ states that the same acoustic pressure disturbance arrives first at one point $\underset{\sim}{x}$ at time t and then at $\underset{\sim}{x} + \underset{\sim}{\xi}$ at a later time $t + \tau$ where $\tau = |\underset{\sim}{\xi}|/c$. The differential correlation function is defined as the contribution from a given unit area on the data plane. If $\underset{\sim}{x}$ and $\underset{\sim}{x} + \underset{\sim}{\xi}$ happen to fall along the path of propagation of the dominant acoustic energy flux coming through this unit area, a significant correlation coefficient can be detected at very large spatial separation distances.

(b) The space-like property refers to the correlation between the simultaneous values of sound pressure at $\underset{\sim}{x}$ and $\underset{\sim}{x} + \underset{\sim}{\xi}$. No cause and effect relation can be established between these points because there is no time for any acoustic signal to travel from one point to another. The linear dependence of the sound pressure between $\underset{\sim}{x}$ and $\underset{\sim}{x} + \underset{\sim}{\xi}$ at $\tau = 0$ is a measure of the inherent similarity of the pressure field. In the present case, the inherent similarity results from the fact that the far-field sound pressure is induced by the coherent acoustic energy flux coming through a unit area of the data plane. Within the space and time framework, the spatial correlation pattern induced by such an apparent sound source propagates outwards in the free space in exactly the same manner as a wave front produced by a deterministic sound source. Such analytical similarity can be verified through the definitions of equations (1) and (2). Based on these reasons, the space-like correlation pattern of the differential correlation function for sound pressure in the far field can be defined as a statistical wave front.

In physical situations, the general behavior of the differential correlation function represents a mixture of the space-like and the time-like properties of the sound-pressure field.

The equivalent sound-source distribution.- Under the Green's function formulation, it is possible to establish an equivalent sound-source distribution by means of a narrow-band spectral analysis. If an apparent sound-source distribution $q(\underset{\sim}{y},t)$ can be assumed in the jet flow, with $q(\underset{\sim}{y},t)$ being a random function, then a cross spectral density function can be defined for the source distribution function, which can be written as

$$S_{qq}(\underset{\sim}{y},\underset{\sim}{\eta},\omega) = \frac{1}{2\pi}\int_{-\infty}^{\infty} e^{-i\omega\tau}\left\langle q(\underset{\sim}{y},t)\; q(\underset{\sim}{y}+\underset{\sim}{\eta},t+\tau)\right\rangle d\tau \tag{4}$$

Similarly, one can define a cross spectral density function in the far field, so that

$$S_{pp}(\underset{\sim}{x},\underset{\sim}{\xi},\omega) = \frac{1}{2\pi}\int_{-\infty}^{\infty} e^{-i\omega\tau} R_{pp}(\underset{\sim}{x},\underset{\sim}{\xi},\tau)\, d\tau \tag{5}$$

The functions $S_{pp}(\underset{\sim}{x},\underset{\sim}{\xi},\omega)$ and $S_{qq}(\underset{\sim}{y},\underset{\sim}{\eta},\omega)$ can be related by means of a double integration formula if the simple wave equation is assumed to hold in spite of the presence of the jet flow. This equation can be written as

$$S_{pp}(\underset{\sim}{x},\underset{\sim}{\xi},\omega) = \frac{1}{(4\pi)^2}\int\int_{V(y),V(\eta)} \frac{1}{r_1 r_2} e^{i\omega(r_1-r_2)/c} S_{qq}(\underset{\sim}{y},\underset{\sim}{\eta},\omega)\, dy^3\, d\eta^3 \tag{6}$$

where

$$r_1 = \left|\underset{\sim}{x} - \underset{\sim}{y}\right|$$

$$r_2 = \left|\underset{\sim}{x} + \underset{\sim}{\xi} - (\underset{\sim}{y} + \underset{\sim}{\eta})\right|$$

The quantities dy^3 and $d\eta^3$ are infinitesimal volume elements, and both of the domains of integration $V(y)$ and $V(\eta)$ are the entire three-dimensional volume over which the apparent source function $q(\underset{\sim}{y},t)$ is defined. The cross spectral density functions in equations (4) and (5) and the Green's function in equation (6) are complex quantities.

Equation (6) is a multidimensional linear relationship between $S_{pp}(\underset{\sim}{x},\underset{\sim}{\xi},\omega)$ and $S_{qq}(\underset{\sim}{y},\underset{\sim}{\eta},\omega)$. In a practical situation, $S_{pp}(\underset{\sim}{x},\underset{\sim}{\xi},\omega)$ rather than $S_{qq}(\underset{\sim}{y},\underset{\sim}{\eta},\omega)$ is more often measurable. It can either be measured directly or derived indirectly from other measurable data. For example, $S_{pp}(\underset{\sim}{x},\underset{\sim}{\xi},\omega)$ can be computed from the space-time correlation function of the normal sound-pressure gradients on the plane mentioned earlier in this section:

$$S_{pp}(\underset{\sim}{x},\underset{\sim}{\xi},\omega) = \frac{1}{4\pi^2}\int\int_{S(y),S(\eta)} \frac{1}{r_1 r_2} e^{i\omega(r_1-r_2)/c} S_{\nabla p \nabla p}(\underset{\sim}{y},\underset{\sim}{\eta},\omega)\, dS(y)\, dS(\eta) \tag{7}$$

with

$$S_{\nabla p \nabla p}(\underset{\sim}{y},\underset{\sim}{\eta},\omega) = \frac{1}{2\pi}\int_{-\infty}^{\infty} e^{-i\omega\tau} R_{\nabla p \nabla p}(\underset{\sim}{y},\underset{\sim}{\eta},\tau)\, d\tau \tag{8}$$

The function $S_{\nabla p \nabla p}(\underset{\sim}{y},\underset{\sim}{\eta},\omega)$ is a cross spectral density function with respect to time variable, and a correlation function in all of the spatial variables. Such a function can be measured directly in an experiment. The function $S_{pp}(\underset{\sim}{x},\underset{\sim}{\xi},\omega)$ evaluated at $\xi = 0$ is proportional to the acoustic energy flux normal to the surface S.

Equation (6) can be considered as a Fredholm integral equation of the first kind if the roles of known and unknown functions are reversed. In the configuration shown in figure 2, the source region and the far field are separated by the plane S; therefore, r_1 and r_2 are always greater than zero. It follows that the kernel function of the Fredholm integral equation is square integrable, and it now appears that this integral equation has a unique solution. This is not the case, however. The unknown function $S_{qq}(\underset{\sim}{y},\underset{\sim}{\eta},\omega)$ depends on six spatial variables, with ω treated as a fixed parameter. The left-hand side of equation (6) also contains six spatial variables. However, equation (7) indicates that $S_{pp}(\underset{\sim}{x},\underset{\sim}{\xi},\omega)$ is actually a function of only four independent spatial variables because each of the $\underset{\sim}{y}$ and $\underset{\sim}{\eta}$ variables on the right-hand side of equation (7) is defined over a two-dimensional surface. A unique solution can be constructed only if additional conditions are known or are imposed upon the unknown source distribution function. In the case of computing an equivalent distribution of apparent sources, these conditions are arbitrary. For example, a unique solution can be obtained from equation (6) if the source function is assumed to be an infinitely thin two-dimensional distribution over a conical surface enclosing the jet flow. The unknown quantity $S_{qq}(\underset{\sim}{y},\underset{\sim}{\eta},\omega)$ in equation (6) is now a function of four variables. Physically, this equivalent sound-source distribution is a two-dimensional image of the actual three-dimensional sound-source distribution within the jet. The sound-source strength is proportional to the acoustic energy flux density passing through the conical surface. Another common assumption is the consideration of the equivalent source as a line distribution along the axis of the jet. This assumption is a special case of the example just given because the axis of the jet can be considered as a degenerated conical surface when the apex angle reduces to zero.

Ray Path Analysis

Instead of analyzing the wave propagation process by means of the Green's function formulation, a study of the delay time relation in the space-time correlation data can provide useful information about the geometrical structure of the acoustic field near the subsonic jet. A correlation function of acoustic signals between a fixed point $\underset{\sim}{x}$ and any given point $\underset{\sim}{x} + \underset{\sim}{\xi}$ is a function of the delay time τ. The geometrical configuration is shown in figure 3, and the definition of correlation functions can be found in equation (2). The delay time at which the correlation function reaches its maximum is designated at τ_{max}. This time of arrival of the maximum correlation value can be interpreted as the difference in time for a statistical wave front emanated from the jet to touch the points $\underset{\sim}{x}$ and $\underset{\sim}{x} + \underset{\sim}{\xi}$. Since such a statistical wave front travels at the speed of sound in the free field, the direction of travel of this statistical wave front can be computed by means of a simple equation:

$$\theta = \cos^{-1}\left(\frac{c\tau_{max}}{d}\right) \tag{9}$$

with

$$d = \left| \underset{\sim}{\xi} \right|$$

where θ is the angle between the direction of the statistical wave front and the line joining the points $\underset{\sim}{x}$ and $\underset{\sim}{x} + \underset{\sim}{\xi}$.

The derivation of equation (9) can be shown in a two-dimensional configuration without loss of generality. Let the statistical wave front be first assumed as a plane. The cosine relation within a right triangle leads to equation (9) and is clearly shown in figure 3. As a second derivation, let the statistical wave front be assumed as spherical. The delay time relation is equivalent to a statement that the difference in distances from the center of the sphere to the points $\underset{\sim}{x}$ and $\underset{\sim}{x} + \underset{\sim}{\xi}$ is a constant. It is known in plane geometry that the locus of the center of the sphere describes a hyperbola. An asymptote to the hyperbola is a straight line passing through the midpoint between $\underset{\sim}{x}$ and $\underset{\sim}{x} + \underset{\sim}{\xi}$ with an inclination defined by the angle θ. In a general three-dimensional situation, the geometrical configuration as described in figure 3 has a rotational symmetry about an axis passing through the points $\underset{\sim}{x}$ and $\underset{\sim}{x} + \underset{\sim}{\xi}$. Hence, the locus of the center of the sphere is a hyperboloid with a conical asymptotic surface. (See sketch in fig. 3.)

The two-dimensional configuration in figure 3 shows that the hyperbolic locus of the center of the sphere comes very close to the asymptote, starting a short distance from the points $\underset{\sim}{x}$ and $\underset{\sim}{x} + \underset{\sim}{\xi}$. Therefore, in this report, the asymptote is termed the ray path, which is a practical approximation to the geometrical acoustic ray representing the local spherical statistical wave front. Although both the plane wave and the spherical wave assumptions lead to the construction of nearly identical ray paths, physical interpretation of the results of subsonic jet noise measurement is much easier with the spherical assumption because it is known that the jet noise source region lies within only a finite distance from the plane of measurement.

DESCRIPTION OF EXISTING DATA

Experimental Setup

A sketch of the experimental setup is shown in figure 4. A subsonic jet was used in the experiment described in reference 5 where the exit diameter was 6.25 cm, the stagnation temperature was ambient, and the exit velocity was 213 m/sec. The boundary of the mixing flow regime was defined as the 1-percent intermittency surface around the jet. This boundary, based on measurements in reference 5, was a conical surface with an half apex angle of 11°. The acoustic measurement was made on a plane near the jet which made an angle of $17^{\circ}20'$ with the axis of the jet. The orientation and the location of the

plane were chosen so that the pressure fluctuations in the neighborhood of the plane were governed by the inverse square law, yet the entire plane remained as close to the jet as possible. Ten stations were chosen on the plane as the reference points for correlation measurements, and their locations are given in table I. The microphone placement around each station was arranged in a polar pattern along radial directions 45° apart. The typical radial separation was 4 cm, with between 75 to 120 points selected at each station. In connection with the present analysis, local Cartesian coordinates are defined so that the origin coincides with the station reference point. As stated in the preceding section, only the local properties of the acoustic data are analyzed, and each station is treated independently. The imaginary data plane serves as the X,Y-plane for the local coordinate system with the X,Z-plane passing through the axis of the jet. The outgoing normal to the plane is designated as the positive Z-axis. This local Cartesian coordinate system serves as either the $\underset{\sim}{x}$ coordinate system in the far field or the $\underset{\sim}{y}$ coordinate system on the data plane. Other details of the experiment can be found in reference 5.

General Characteristics of the Data

The pressure gradient normal to the plane was directly measured by using an electret pressure-gradient microphone (ref. 5). Since the linear response of this transducer was restricted in frequency, the data are prefiltered to within a band from 250 to 3000 Hz. The peak frequency of the jet is close to 1000 Hz; hence, approximately one and one-half octaves on either side of the peak of the jet noise spectrum are included in the data. Cross correlation functions for the prefiltered signal from pairs of microphones were obtained by using a real-time correlator. All of the cross correlation functions were taken with a 20-microsecond time delay interval with a few exceptions where a 50-microsecond time interval was used. Typical sets of the correlation function are shown in figures 5, 6, and 7.

These figures show the values of the space-time correlation function $R_{\nabla p \nabla p}(0,\underset{\sim}{\eta},\tau)$ as a function of the spatial separation vector and the delay time τ. The first variable in the correlation function is zero because the reference point of correlation is chosen as the origin of the local coordinate system. The result of measurement at station 1 is shown in figure 5. Three groups of curves are in this figure with the direction of the spatial separation vector $\underset{\sim}{\eta}$ fixed in each group. Hence, an individual curve represents the variation of $R_{\nabla p \nabla p}(0,\underset{\sim}{\eta},\tau)$ as a function of τ at a given value of the separation distance η along the given direction of the group. Beyond a certain value of spatial separation, the value of the cross correlation function ceased to maintain any significant value, at which point the series of measurements would terminate. Such maximum distance of correlation can be referred to as the range of correlation. Incidentally, the maximum correlation amplitude at large values of η occurs also at a large value of τ. Hence, a group of correlation function curves which has a large correlation range in the

spatial domain also has a large correlation range in the time domain. The group of correlation curves with the spatial separation in the Y-direction in figure 5 are given only for positive values of η. Measurements in reference 1 had shown that the correlation patterns were symmetric with respect to the X,Z-plane. For the data at station 1, the correlation range for each of the chosen directions is approximately the same. As measurement proceeded from one station to another, the correlation range in the Y-direction remained approximately the same; however, the correlation range changed significantly in the X-direction. Figure 6 shows three groups of correlation curves with separation distances in the X-direction for stations 3, 5, and 7. The range of correlation increases progressively from the upstream stations to the downstream stations. Figure 7 shows the entire set of data from station 9. The great disparity of correlation range in the X-direction and the Y-direction can easily be noted. Significant correlation values remain observable for separation distances of more than 15 diameters along the positive X-axis. The continual elongation of the X-direction correlation range can be explained later in this paper when the concept of beam pattern radiation of jet noise is introduced.

Although the above-mentioned figures contain sufficient information to describe the propagation of sound near the jet, these figures lack the ability to convey an intuitive visual impression to the reader. There is a better way of data presentation for the purpose of visualization. The correlation function can be given in terms of spatial contours at a fixed value for delay time. The data set, as obtained at station 8, is presented in the form of such spatial contours in figure 8. This figure contains four sets of spatial contours at τ = -0.2, 0.0, 0.6, and 1.4 milliseconds shown from left to right in the order of increasing delay time. This figure shows contours which represent negative values of the correlation function as dotted lines. If each set of spatial contours of the correlation function is considered as a statistical wave front (discussed in the previous section), then figure 8 illustrates the propagation of such a statistical wave front from upstream to downstream along the data plane. The center of the statistical wave front touches the origin of the local coordinate system at τ = 0. The shape of the statistical wave front appears to spread out and form a circular arc as the delay time approaches larger values.

DISCUSSION OF RESULTS

Sound-Source Location

Construction of the ray bundle.- The method of ray path analysis is a simple way to find the apparent sound-source location by means of the measured space-time correlation function of the normal sound-pressure gradient on an imaginary plane near the subsonic jet. For data sets such as those shown in figures 5 and 7, one geometrical acoustic ray can be constructed from each time correlation function at a given spatial separation. All the rays at one station form a bundle. The ray bundles at stations 3 and 8 are shown in

figures 9 and 10, respectively. Figure 9 shows the rays reconstructed at points along the X-axis and the Y-axis in the local coordinates at station 3. For the bundle along the X-direction, the rays converge to a very small region within the jet directly opposite to the location of station 3. The bundle along the Y-direction also has a remarkably sharp convergence to a small region. These two bundles can be fitted together to form a three-dimensional bundle which is illustrated by the sketch in figure 9. Only the ray bundle along the X-direction is shown in figure 10. In this case, the bundle converges to a somewhat larger region in the jet. Figure 10 demonstrates the significant point that the location of the apparent source region within the jet is far upstream from the reference point at station 8. Table I shows that station 8 is located at 16.65 diameters downstream from the nozzle exit, while the average location of the apparent source region is approximately 8.8 diameters from the nozzle exit.

As these figures show, there is some random deviation in the ray direction. Only the average direction of the ray bundle is meaningful. After constructing all the ray bundles for all the stations, parameters related to the geometrical configuration of the ray bundles (average direction, average location, and approximate length of the region of convergence, etc.) have been obtained and are summarized in table I. Figure 11 shows the average ray bundle direction for all the stations and the outline of the ray bundle for every third station. It is obvious from this figure that there is continuous variation of the noise emission pattern from different parts of the jet mixing flow.

For each of the 10 stations the ray bundle converges to a relatively small region in the jet flow. The convergence is a strong indication that the dominant part of the acoustic energy reaching the plane of measurement originates from small volumes of coherent random sound sources. A quantitative analysis of the apparent source strength distribution for each of the ray bundles can be done, in principle, according to earlier discussions concerning the Green's function formulation. However, such an analysis is not included in this study; an indirect estimate of the apparent source strength distribution is discussed in the following section.

In reference 6, Maestrello and McDaid analyzed the narrow-band acoustic energy flux vectors near a subsonic jet according to measurements obtained in the neighborhood of one reference point. The reader may be interested in referring to this previous work for comparison with the present results.

Comparison with the mirror technique.- The normal acoustic energy flux along the plane of measurement was previously computed in reference 5 based on the experimental values of $R_{\nabla p \nabla p}(\underset{\sim}{y},\underset{\sim}{\eta},\tau)$. With a further assumption of symmetry about the axis of the jet, the apparent source strength distribution per unit length of the jet was computed by multiplying the acoustic energy flux density by the area of a ring segment of the conical surface which is generated by rotating the plane of measurement around the axis of the jet.

Figure 12 shows the results of the power per unit length normalized against the total power of the jet and plotted against the Strouhal number. The peak amplitude occurs at $fD/U_j = 0.3$, and it is in good agreement with the commonly measured peak value of the far-field jet noise spectrum. In the spatial coordinate, the variation of the apparent source strength is very gradual except for the initial few diameters. The peak apparent source strength per unit length of the jet occurs at approximately 9 diameters downstream. However, such apparent source strength distribution is obtained according to the normal acoustic energy flux at the plane of acoustic measurement. If the vectorial property of the acoustic energy flux is considered, the location of the apparent source should be shifted from its location along the plane to its apparent location along the axis of the jet. The shift can best be made by following the average direction of the ray bundle. The shifted apparent source strength distribution has an important advantage: it is independent of the position of the plane of acoustic measurement. For example, if a shift is applied to the source distribution of figure 12, the point of maximum strength is located at approximately 6.6 diameters downstream from the nozzle exit of the jet.

It is interesting to compare the result of this study with the mirror technique as recently described by Grosche, Jones, and Wilhold (ref. 3) and by Laufer, Schlinker, and Kaplan (ref. 4). The mirror is a high-gain, direction-sensitive device which has a large aperture to receive the acoustic signal from the jet. The measured signal represents the radiated sound from a small volume of the flow which is located at one focal point of the mirror. On the other hand, the technique described here for measuring the space-time correlation function of the normal sound-pressure gradient on a plane can record the phase and amplitude of the acoustic signal as emitted from the jet over a large area on the plane of measurement. The analysis of such data by means of either the delay time technique or the Green's function formulation can reconstruct the acoustic image of the apparent sound source. Hence, the results produced by the present technique and those produced by the mirror technique are similar in nature. The relative advantages and drawbacks for these two techniques should be an important subject for further studies.

Additional evidences of sound-source localization.- Some supplemental experimental data are available to support the hypothesis that a coherent volume of random sound sources within the jet is highly localized. These data include measurements made inside and immediately outside the shear layer of the jet. Within the shear layer, a set of hot-wire anemometers with standard signal conditioning devices to discriminate between turbulent and nonturbulent regions was used; outside the shear layer a pair of microphones were chosen for pressure measurements. The hot wires were placed around the circumference of the jet at the radial distance where the intermittency value was $\gamma = 0.5$. The radial component of the velocity field thus obtained can be considered as the radial component of the local vorticity according to Corrsin and Kistler (ref. 7). Hence, the resultant spatial correlation $R\left(\phi^*, x_j/D\right)$ can be interpreted as the spatial correlation of the

radial vorticity component about a radius where the mean intermittency signal is 50 percent turbulent. Such data were taken at two stations downstream of the nozzle at $x_j/D = 4$ and $x_j/D = 8$; the results are shown in figure 13.

The correlation is of appreciable amplitude only over azimuth angles of about 10^o in either the $+\phi^*$ or $-\phi^*$ directions. Although this result does not describe a complete source element in the jet, it does support the view that the true sources are localized and uncorrelated over large azimuthal angular separations. This result again supports the view that localized sources in the flow produce the sound field.

Immediately outside the jet, the pressure fluctuations can be thought of as associated with the vorticity in the flow. Microphone correlation measurements over ϕ^* for $x_j/D = 2$ and $x_j/D = 4$ are shown in figure 14. At 90^o, the correlation level drops to 0.4 of the peak value, and becomes very small beyond 120^o. It is not surprising that the pressure correlates over a greater angle because the microphones may receive signals from sources at a distance, where the propagation effects naturally broaden the correlation distance. One interesting aspect of the pressure measurement is that the peak of correlation for all angles occurs at zero time delay. This evidence tends to rule out the possibility of dominant spiral modes in the flow. In a recent paper by Michalke and Fuche (ref. 8), similar observations and conclusions were reported. Additional evidence that the pressure about the jet is not fully correlated around the circumferential direction was reported by Liu, Maestrello, and Gunzburger (ref. 9).

Statistical Nature of the Sound Field

The far-field distribution of the mean square sound pressure.- A highly descriptive numerical result is the distribution of $D\left[R_{pp}(\underset{\sim}{x},0,0)\right]$ in the far field. The result is the mean square pressure distribution as induced by the acoustic energy flux coming through a unit area on the data plane at a reference station. The contour plots of $D\left[R_{pp}(\underset{\sim}{x},0,0)\right]$ in the X,Z-plane for all the odd number stations are shown in figure 15. The values of the contour are given in physical units, and the coordinates are given in terms of X/D and Z/D. The general direction of wave propagation agrees very well with the ray path analysis. If the sound wave passing through each station is assumed to originate from the tip of the corresponding ray bundle, the distribution of $D\left[R_{pp}(\underset{\sim}{x},0,0)\right]$ follows the inverse square law rather accurately.

In a previous paper describing the initial results of this study (ref. 1), some negative values of $D\left[R_{pp}(\underset{\sim}{x},0,0)\right]$ were noted in the computed results following directly from the application of equation (3). An example is shown in figure 16. There are two possible causes for the presence of such negative values:

(a) The value of $D\left[R_{pp}(\underset{\sim}{x},0,0)\right]$ is a summation over all the data at each station. Theoretically, the integral should always have a positive value. If the data are imperfect, the numerical integrations need not be positive.

(b) The acoustic signal is taken within a frequency band of approximately one decade. The phase effect of such data may have resulted in the appearance of the negative loops.

Further investigation into the numerical details revealed that the actual value of $D\left[R_{pp}(\underset{\sim}{x},0,\tau)\right]_{\tau=0}$ is shifted slightly in time. The average time shift is approximately 120 microseconds, while the actual value depends on the radial distance of the point under consideration. A typical example is shown in figure 17. Such a time shift is very probably a direct result of data imperfection compounded by the strong modulation of the correlation function which was caused by the band limitation of the original acoustic signal.

The direction of flow of the dominant portion of acoustic energy can be determined roughly from the distribution of $D\left[R_{pp}(\underset{\sim}{x},0,0)\right]$. On a point-by-point basis, the local wave propagation direction can be determined rigorously by computing the maximum of the local pressure-gradient correlation function. An integral formula for such computation can be readily derived from equations (1) and (2) by differentiating the entire equation with respect to the direction of the desired component of pressure gradient. However, the formula would involve a second time derivative of the function $R_{\nabla p \nabla p}(\underset{\sim}{y},\underset{\sim}{\eta},\tau)$ which is a measured quantity. Hence, the numerical accuracy of such computation is questionable.

The correlation relations of sound pressure in the far field.- The cross correlation function of sound pressure provides a quantitative measure of the linear dependence of the acoustic signal at different points. The normalized form of the differential cross correlation function provides a convenient way to study the statistical structure of the induced sound-pressure field. The normalization can take two different forms:

$$\rho_0(\underset{\sim}{x},\underset{\sim}{\xi},\tau) = \left\{D\left[R_{pp}(\underset{\sim}{x},0,0)\right]\right\}^{-1} D\left[R_{pp}(\underset{\sim}{x},\underset{\sim}{\xi},\tau)\right] \tag{10}$$

and

$$\rho_1(\underset{\sim}{x},\underset{\sim}{\xi},\tau) = \left\{D\left[R_{pp}(\underset{\sim}{x},0,0)\right] D\left[R_{pp}(\underset{\sim}{x}+\underset{\sim}{\xi},0,0)\right]\right\}^{-1/2} D\left[R_{pp}(\underset{\sim}{x},\underset{\sim}{\xi},\tau)\right] \tag{11}$$

The first definition is a normalization of the differential correlation amplitude with respect to its maximum value at the reference point. The second definition has taken into account the local maximum amplitude at both points as involved in the cross correlation. The second definition is preferred from a physical standpoint.

A typical set of reconstructed differential correlation functions are shown in figure 18, which are based on the data at station 5. The reference point and the variable

point are confined to the X,Z-plane. The moving spatial point is taken along a line perpendicular to the direction as defined by the origin of the local coordinate and the reference point. The geometrical configuration is shown in a sketch in figure 19.

Since the wave propagation process becomes self-similar in the far field along the radial direction in a spherical coordinate system, the spatial distribution of the differential correlation coefficient can best be described in such a coordinate system (fig. 19). Consider the case of a reconstructed differential correlation function where both the reference point and the moving point are confined to a spherical coordinate surface. The spatial separation can then be described in the angular coordinates ψ and ϕ. In many of the computations, the correlation coefficient is computed along lines tangent to the sphere at the reference point. The correspondence between the angular coordinate ϕ and the linear separation distance can be given simply by:

$$\tan \phi = \frac{d}{R} \qquad d = \left| \underset{\sim}{\xi} \right| \tag{12}$$

An inverse square law correction factor must be applied to the differential correlation coefficient $\rho_0(\underset{\sim}{x},\underset{\sim}{\xi},\tau)$ when the description is transferred from the tangent to the spherical surface:

$$\rho_0(\underset{\sim}{x},\phi,\tau) = (\cos \phi)^{-1} \rho_0(\underset{\sim}{x},\underset{\sim}{\xi},\tau) \tag{13}$$

The value of $\rho_1(\underset{\sim}{x},\underset{\sim}{\xi},\tau)$ remains unchanged for the same coordinate transfer.

Values of $\rho_0(\underset{\sim}{x},\phi,\tau)$ and $\rho_1(\underset{\sim}{x},\phi,\tau)$ are computed at all of the stations. The reference point of correlation is typically chosen at a distance 100 diameters away from the origin and along the average outgoing direction of the ray bundle at this station. For each given value of ϕ the correlation coefficient reaches a maximum at a certain delay time τ_{max}. The envelope of such maximum values provides a measure of the width in the sound field over which the sound-pressure field fluctuations remain linearly dependent. Note that the boundary of correlation is now expressed in angular coordinates. As long as the reference point is chosen along the average ray bundle direction and the radius is very large, the values of $\rho_0(\underset{\sim}{x},\phi,\tau_{max})$ and $\rho_1(\underset{\sim}{x},\phi,\tau_{max})$ are invariant. Hence, the domain of correlated sound propagation is in the pattern of a narrow beam as confined within a conical surface. A detailed discussion of the beam pattern concept is given in the following section.

Both $\rho_0(\underset{\sim}{x},\phi,\tau_{max})$ and $\rho_1(\underset{\sim}{x},\phi,\tau_{max})$ are rapidly decreasing functions of ϕ. The actual dependence varies from station to station. The results are summarized in figures 20 and 21. In these figures, the average is shown in circles and the maximum range of variation of the differential correlation coefficients is shown by means of a line

interval. A curve for $\cos^4 \phi$ is shown in both figures for comparison. This particular function was chosen because it represents the directivity of an idealized quadrupole. Figure 20 shows that the average shape of $\rho_0(\underset{\sim}{x},\phi,\tau_{max})$ is substantially narrower than $\cos^4 \phi$. The angular span between the points where the differential correlation coefficient reaches 0.5 is approximately 25^o. Figure 21 shows that the value of $\rho_1(\underset{\sim}{x},\phi,\tau_{max})$ initially follows the $\cos^4 \phi$ curve, but then it goes above this curve for larger values of ϕ. The angular span between the points $\rho_1(\underset{\sim}{x},\phi,\tau_{max}) = 0.5$ is approximately 35^o.

A particular set of computations based on the data at station 8 was obtained in order to show the statistical structure of the pressure field on a plane which is perpendicular to the average ray bundle direction. At station 8, the average direction of the ray bundle is 33^o from the data plane. The reference point of correlation is chosen as 100 diameters away from the origin. The plane in which $\underset{\sim}{\xi}$ varies is tangent to the coordinate sphere passing through the reference point. Local coordinates are given on this plane in order to fix its orientation with respect to the Cartesian coordinate system at station 8. The X'-axis lies within the X,Z-plane, and it points in the general downstream direction of the jet. The Y'-axis is normal to the X,Z-plane. In figure 22, two groups of curves are shown. At each point in this plane, the maximum correlation amplitude arrives at a specific delay time τ_{max}. The contours of constant time of arrival are given as the dashed lines in figure 22. Note that this group of contours forms a set of almost perfect concentric circles around the origin. This formation is typical of the traces produced by the passage of a spherical wave front through the plane. In particular, the direction of propagation is perpendicular to this X',Y'-plane. The other set of contours, as shown in solid lines, denotes the distribution of the maximum value of the differential correlation function $D\left[R_{pp}(\underset{\sim}{x},\underset{\sim}{\xi},\tau)\right]$. This second set of contours shows that the amplitude of correlation is directionally dependent. In general, the correlation amplitude decreases rapidly with increasing spatial separation in the X'-direction; such a decreasing trend is somewhat slower in other directions on the plane.

Figure 23 shows another view of $D\left[R_{pp}(\underset{\sim}{x},\underset{\sim}{\xi},\tau)\right]$ in the far field. The differential correlation function is computed with a fixed reference point A and a fixed delay time $\tau = 1.0$ millisecond. The value of $\underset{\sim}{\xi}$ is restricted to the X,Z-plane within an annular sector as shown by the heavy dashed line in figure 23. As previously discussed, the spatial correlation contours can be considered as a statistical wave front. In this case, the statistical wave front is induced by the acoustic energy flux from a unit area on the data plane. Since the point A is chosen as the reference point, this statistical wave front reaches A at $\tau = 0$. It moves away into the far field as τ increases. The arc F-F would indicate the position of the correlation contour pattern if it is computed at a delay time somewhat greater than 1.0 millisecond. The average position of this correlation contour pattern is approximately 35 diameters away from station 8. Remarkably, its shape is nearly

circular within a short distance from the jet flow. This is a strong indication that coherent sound sources in the jet are highly localized.

The beam pattern concept.- The above analysis allows a number of new features of jet noise mechanisms to be confirmed. First of all, the location of the apparent sound sources can be determined accurately. The source region within the jet responsible for the emission of correlated sound in the far field appears to be highly localized. Furthermore, the sound pressure in the far field is correlated within a narrow conical domain. This domain can be referred to as a beam pattern. This use of the term "beam pattern" differs from conventional usage where the width of the beam is normally defined according to the acoustic intensity. In the present case, the statistical beam width is defined according to the value of the differential correlation coefficient across the beam.

Both the correlation measurements and the statistical properties derived from the data provide strong evidence that some order does exist in the random acoustic field near a subsonic jet. Since assumptions drastically contrary to existing theories of jet noise are unnecessary, the following physical model of subsonic jet noise radiation can be postulated.

Jet noise is radiated from localized volumes of correlated turbulence within the jet flow. Within a given short period of time, the coherent noise radiation is pointed mainly in one direction in the fashion of a narrow beam. However, the direction of the beam from such a radiating volume is random in time. Therefore, the commonly measured smooth directivity pattern is an envelope of a large number of such narrow beams.

The time randomness of the beam pattern is simply a reminder of known properties of turbulence. Since the correlation functions are measured by means of a time averaging process, the time randomness property is not distinguishable in experimental measurements. It is important to point out such a possibility since the common emphasis in the literature for the purpose of explaining the structure of the acoustic far field is placed on the spatial randomness of the distribution of turbulence. With the assumption of time randomness, the size of the spatially coherent sound-source volume can either be large or small while the overall directivity as produced by such sound sources can remain compatible with known experimental evidences.

Such a description of jet noise radiation mechanism is also consistent with the concept of a turbulent quadrupole. In jet noise theories, the overall contribution from all components of the quadrupole tensor to a point in the far field is equivalent to a single longitudinal quadrupole pointing in the direction of the receiver. As the data analysis has shown, the directivity of the narrow beam pattern is indeed close to the shape of $\cos^4 \phi$.

An immediate application of the beam pattern concept is the provision of a physical interpretation of the properties of the original space-time correlation data of the normal

sound-pressure gradient on a plane near the jet. For the upstream stations, the direction of the beam pattern is almost perpendicular to the plane. Hence, the correlation patterns on the plane represent the relatively short space-like correlation range across the narrow beam. For the downstream stations, the direction of the beam makes a very small angle with the surface of the plane. The statistical wave front within the narrow beam propagates from one end of the plane to another sweeping out into a much elongated correlation pattern along the X-direction.

The beam pattern concept together with the methods of analysis described in this study should aid the development of techniques to observe further details of the sound-source structure within the jet.

CONCLUDING REMARKS

By using a new approach in analysis, the information retrieved from measured space-time correlation functions of the normal sound-pressure gradient on an imaginary plane near a subsonic jet has suggested the following conclusions:

1. The apparent origin of coherent sound emission within the jet flow is localized.

2. The apparent sound-source location can be determined accurately by reconstructing a geometrical acoustic ray bundle at each station of acoustic measurements. Each of the ray bundles converges to a specific region in the jet flow. The average direction of the ray path varies continuously from station to station. The most important conclusions here are: (a) in the near field, the acoustic energy flux is not normal to the jet boundary, and (b) the apparent sound-source locations in the jet may lie at a point significantly far upstream from the reference point where the acoustic measurements were made.

3. Within the reconstructed sound-pressure field far away from the plane of measurement, the sound pressure is correlated only between points confined within a conical region surrounding the average direction along which the dominant portion of the acoustic energy flux is transmitted. The reconstructed sound-pressure distribution mentioned above is induced by the acoustic energy flux passing through a unit area on the data plane. The distribution of the correlation coefficient within this conical region is very similar to one produced by a longitudinal quadrupole pointing along the axis of the conical region.

4. The definition of the reconstructed sound-pressure field permits the spatial contours of the reconstructed differential correlation function to be considered as a statistical wave front. The computed motion of such statistical wave fronts can provide valuable insight into the process of sound propagation near the jet.

5. A physical model of subsonic jet noise radiation can be postulated according to the observable mechanisms of jet noise emission as obtained in this study. Jet noise is

radiated from localized volumes of correlated turbulence within the jet flow. Within a given short period of time, the coherent noise radiation is pointed mainly in one direction in the fashion of a narrow beam. However, the direction of the beam from such a radiating volume is random in time. Therefore, the commonly measured smooth directivity pattern is an envelope of a large number of such narrow beams.

Since the data of the space-time correlation measurement cover 10 stations located between 0 to 20 diameters downstream from the nozzle exit, continuous variation of the local noise emission pattern along the jet is clearly visible from the reconstructed information concerning the sound field. The present technique of analysis has proven to be a dependable practical method for comprehensive studies of sound emission mechanisms in the noise production region of the jet.

Langley Research Center
National Aeronautics and Space Administration
Hampton, Va. 23665
December 5, 1975

REFERENCES

1. Pao, S. Paul; and Maestrello, Lucio: New Evidence of Subsonic Jet Noise Mechanisms. AIAA Paper No. 75-437, Mar. 1975.

2. Maestrello, Lucio; and Pao, S. Paul: New Evidence of the Mechanisms of Noise Generation and Radiation of a Subsonic Jet. J. Acoust. Soc. America, vol. 57, no. 4, Apr. 1975, pp. 959-960.

3. Grosche, F. R.; Jones, J. H.; and Wilhold, G. A.: Measurements of the Distribution of Sound Source Intensities in Turbulent Jets. AIAA Paper No. 73-989, Oct. 1973.

4. Laufer, J.; Schlinker, R.; and Kaplan, R. E.: Experiments on Supersonic Jet Noise. AIAA Paper No. 75-478, Mar. 1975.

5. Maestrello, Lucio: On the Relationship Between Acoustic Energy Density Flux Near the Jet Axis and Far-Field Acoustic Intensity. NASA TN D-7269, 1973.

6. Maestrello, L.; and McDaid, E.: Acoustic Characteristics of a High-Subsonic Jet. AIAA J., vol. 9, no. 6, June 1971, pp. 1058-1066.

7. Corrsin, Stanley; and Kistler, Alan L.: Free-Stream Boundaries of Turbulent Flows. NACA Rep. 1244, 1955. (Supersedes NACA TN 3133.)

8. Michalke, A.; and Fuche, M. V.: Description of Turbulence and Noise of an Axisymmetric Shear Flow. DLR FB 74-50, July 12, 1974.

9. Liu, C. H.; Maestrello, L.; and Gunzburger, M. D.: Simulation by Vortex Rings of the Unsteady Pressure Field Near a Jet. AIAA Paper No. 75-438, Mar. 1975.

TABLE I.- STATION COORDINATES AND THE LOCATION OF APPARENT SOURCES

Station number	0	1	2	3	4	5	6	7	8	9
Location:										
x_j/D	0.0	0.945	1.87	3.72	5.54	7.42	9.25	12.98	16.65	20.56
r/D	5.0	5.29	5.58	6.16	6.73	7.32	7.88	9.05	10.20	11.42
Average ray direction	98^o	99^o	100^o	99^o	89^o	82^o	72^o	59^o	51^o	47^o
Width of ray bundle	33^o	34^o	35^o	32^o	34^o	40^o	26^o	24^o	17^o	14^o
Apparent source region centered at x_j/D	0.8	1.4	2.4	4.8	5.7	6.4	6.8	8.3	8.8	9.5
Length, $\Delta x_j/D$ . .	1.0	1.5	2.0	1.2	1.0	1.3	2.0	2.5	3.0	3.0

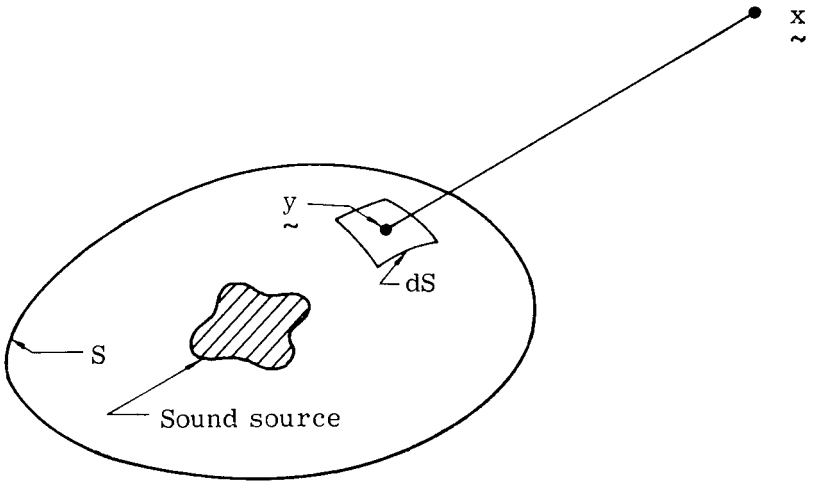

Figure 1.- Sketch for the general Green's function formulation.

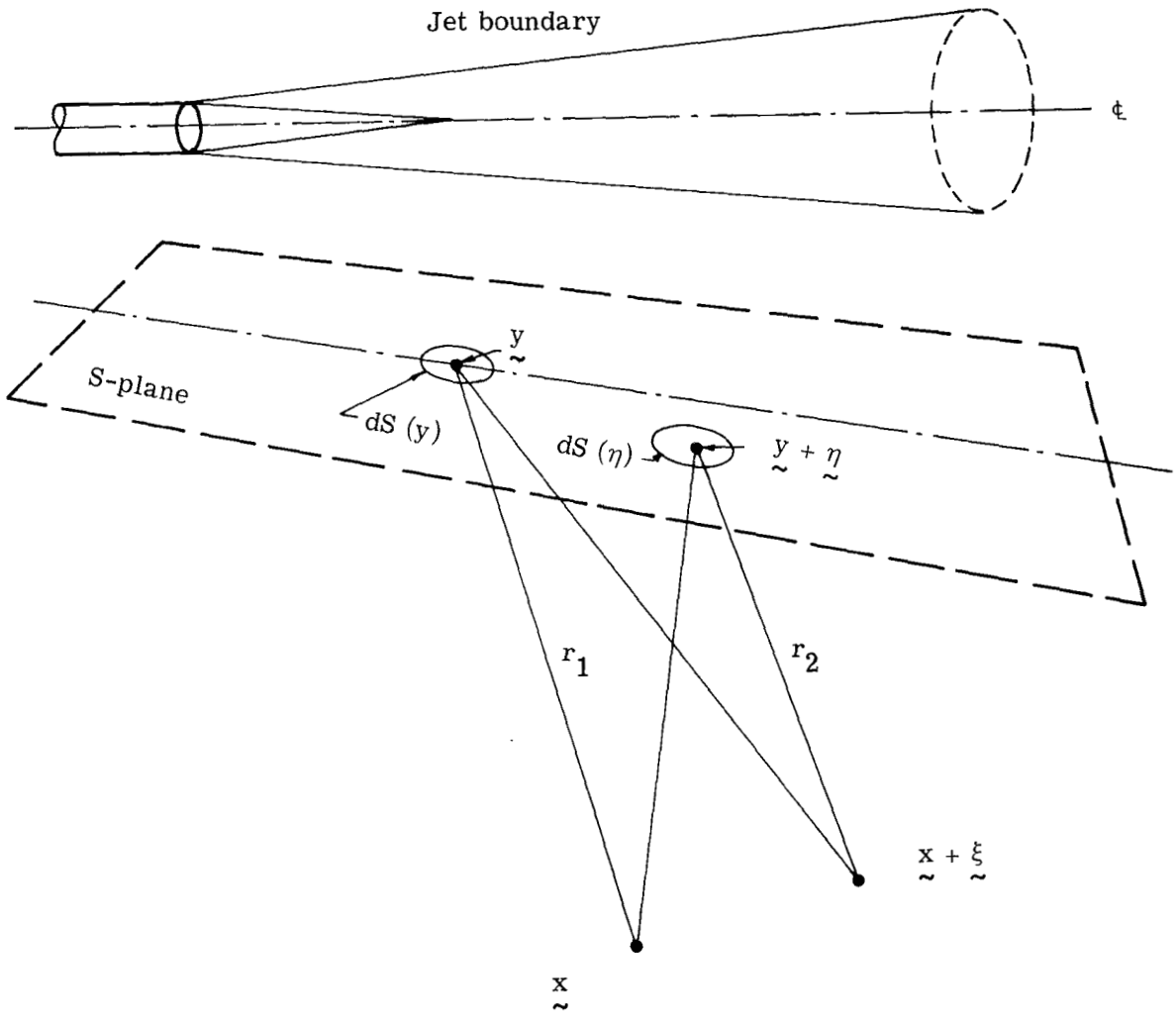

Figure 2.- Sketch for the Green's function formulation for this study.

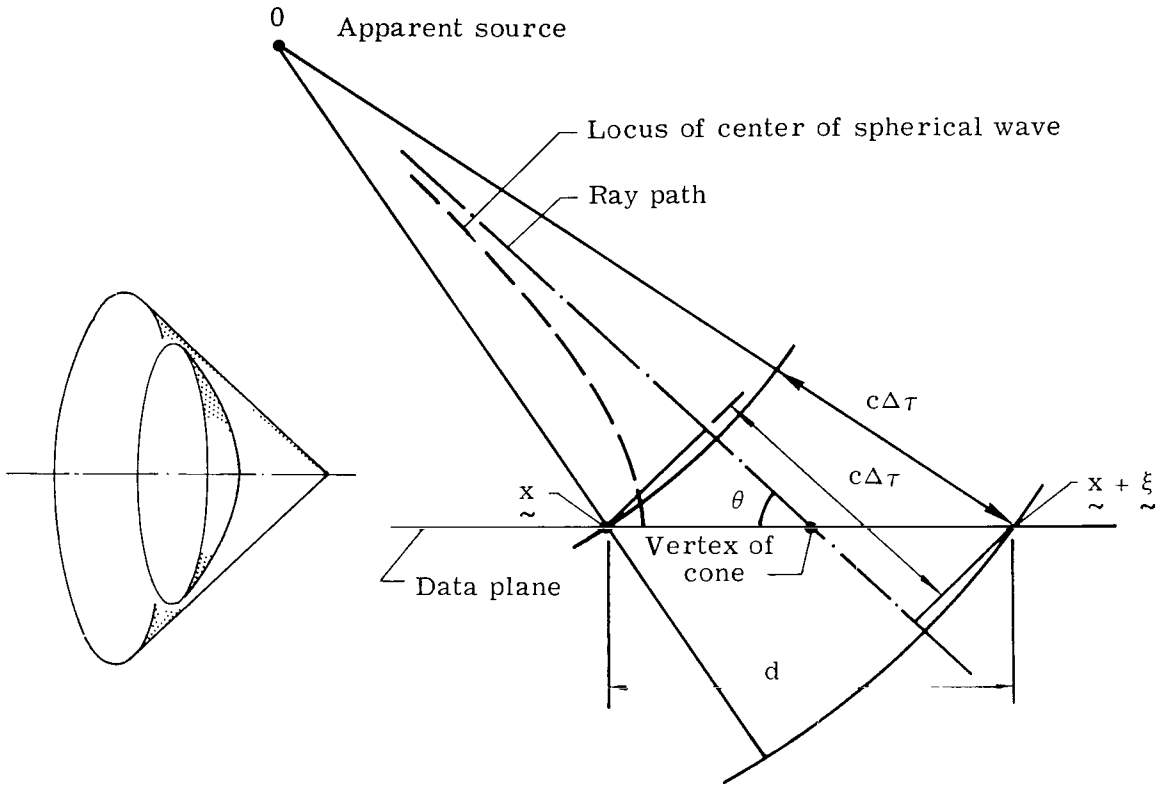

Figure 3.- Sketch of ray path reconstruction.

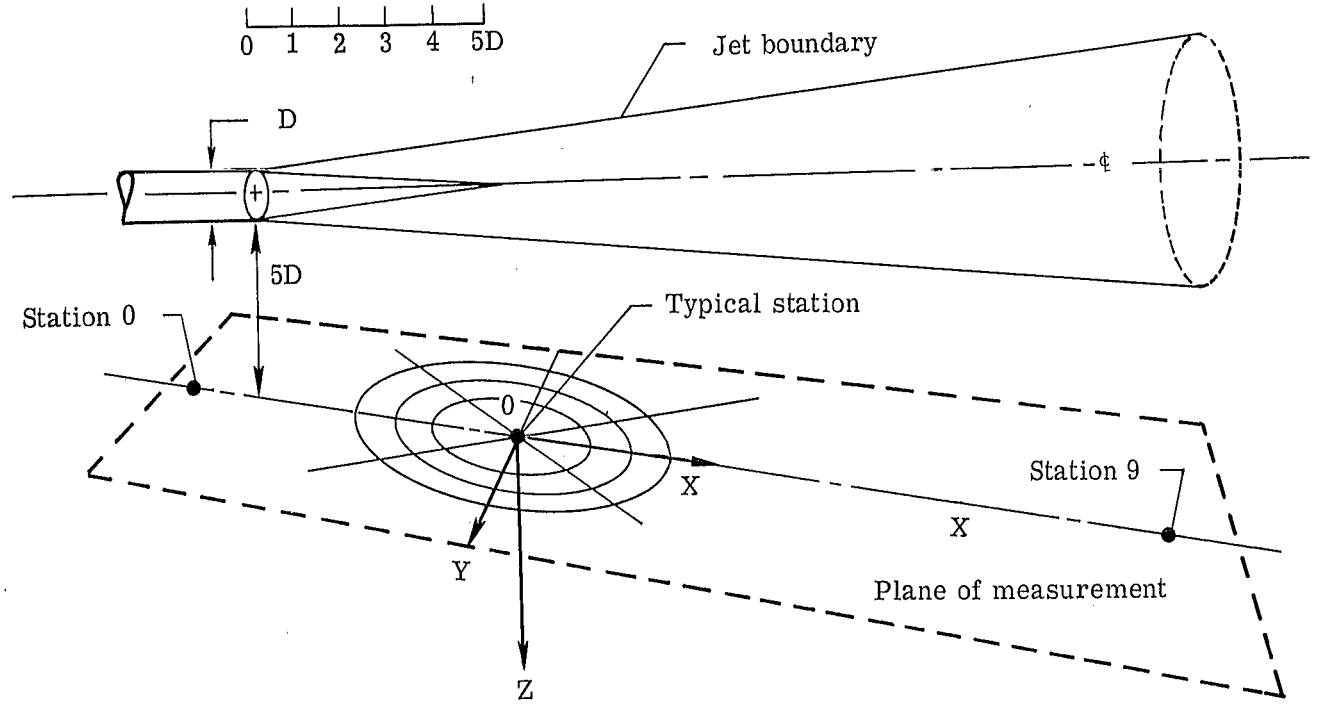

Figure 4.- Setup of pressure-gradient microphone measurements near subsonic jet.

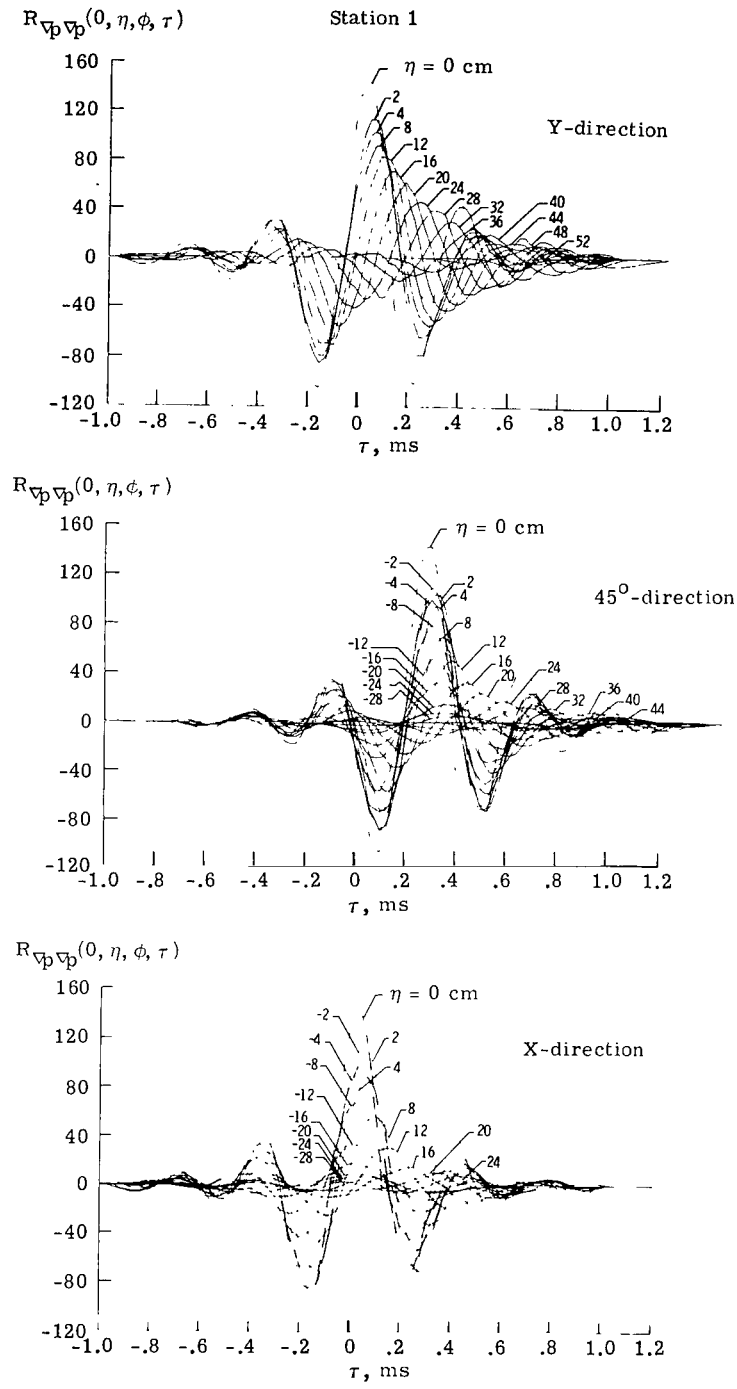

Figure 5.- Space-time correlation functions of the sound-pressure gradient at station 1. Spatial separation η is measured along (a) Y-axis; (b) 45°-direction; and (c) X-axis. Units are measured in 10^{-10} N^2/cm^6.

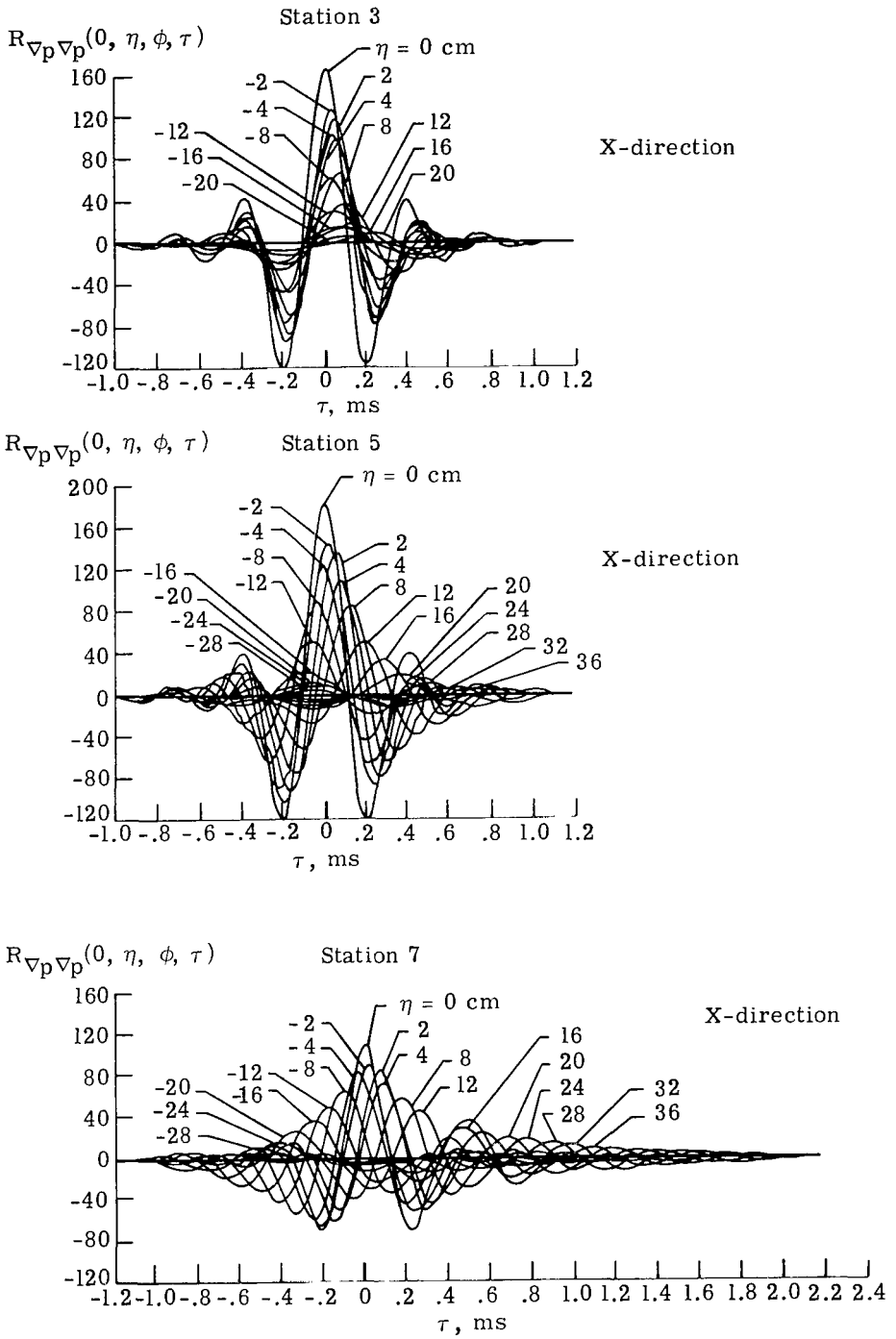

Figure 6.- Evolution of space-time correlation function from station 3 to station 7. The spatial separation is measured along the X-axis. Units are measured in 10^{-10} N^2/cm^6.

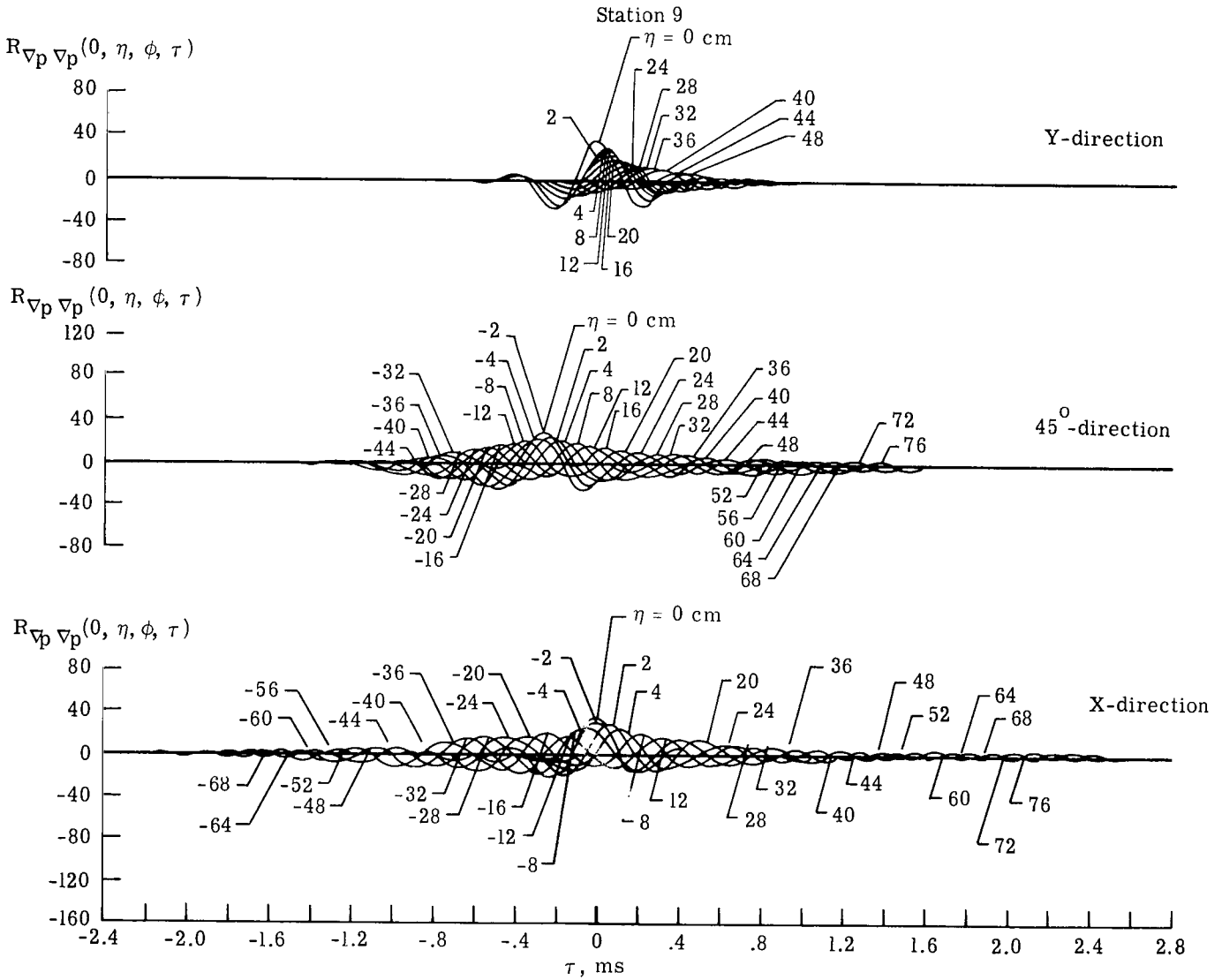

Figure 7.- Space-time correlation functions of sound-pressure gradient at station 9. Spatial separation η is measured along (a) Y-axis; (b) 45^{o} ray; and (c) X-axis. Units are measured in 10^{-10} N^2/cm^6.

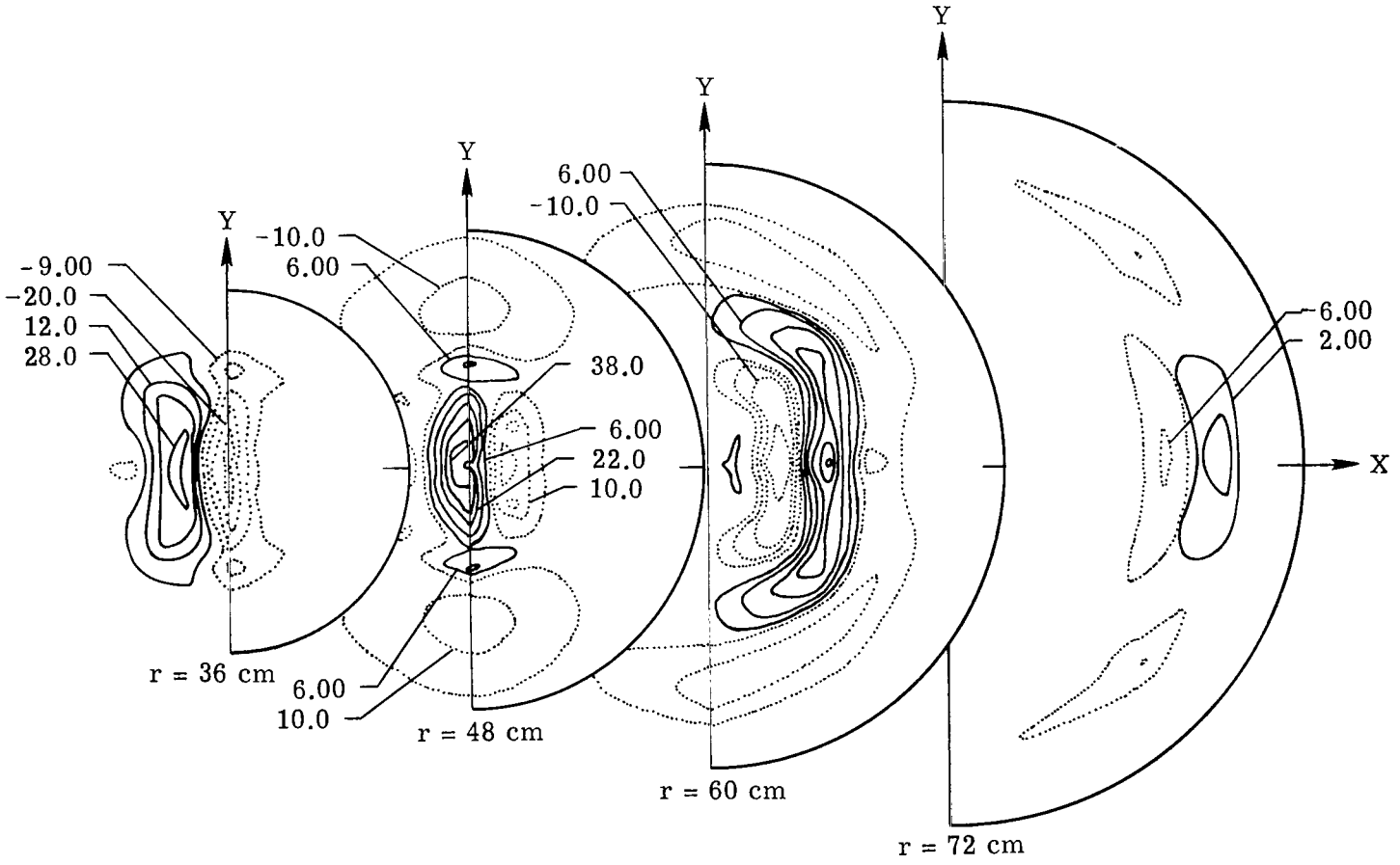

Figure 8.- Contours of equal sound-pressure gradient correlation on data plane at station 8. Contours are shown at four time delays τ = -0.2, 0.0, 0.6, and 1.4 ms. Units are measured in 10^{-10} N^2/cm^6.

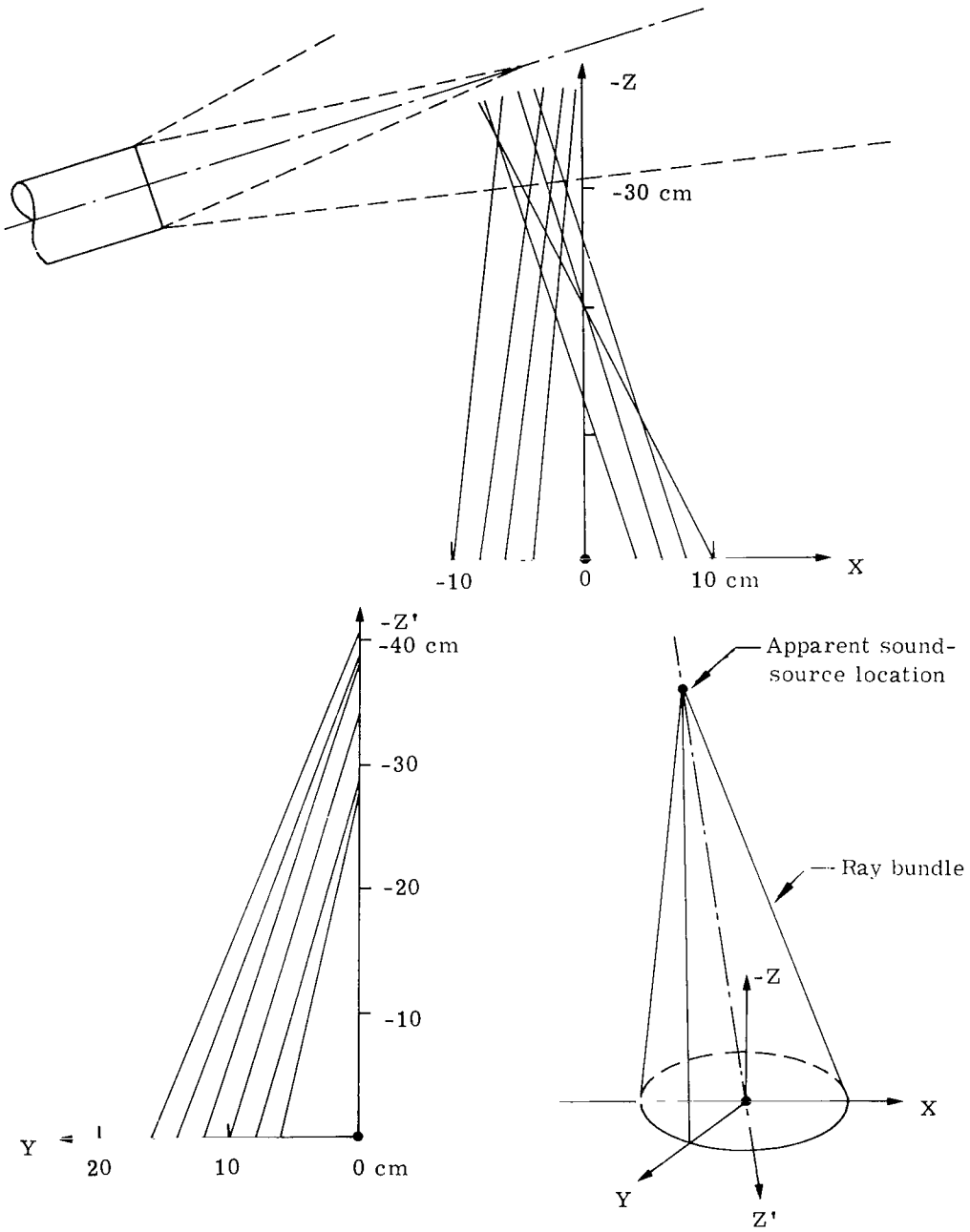

Figure 9.- Ray bundle reconstruction at station 3.

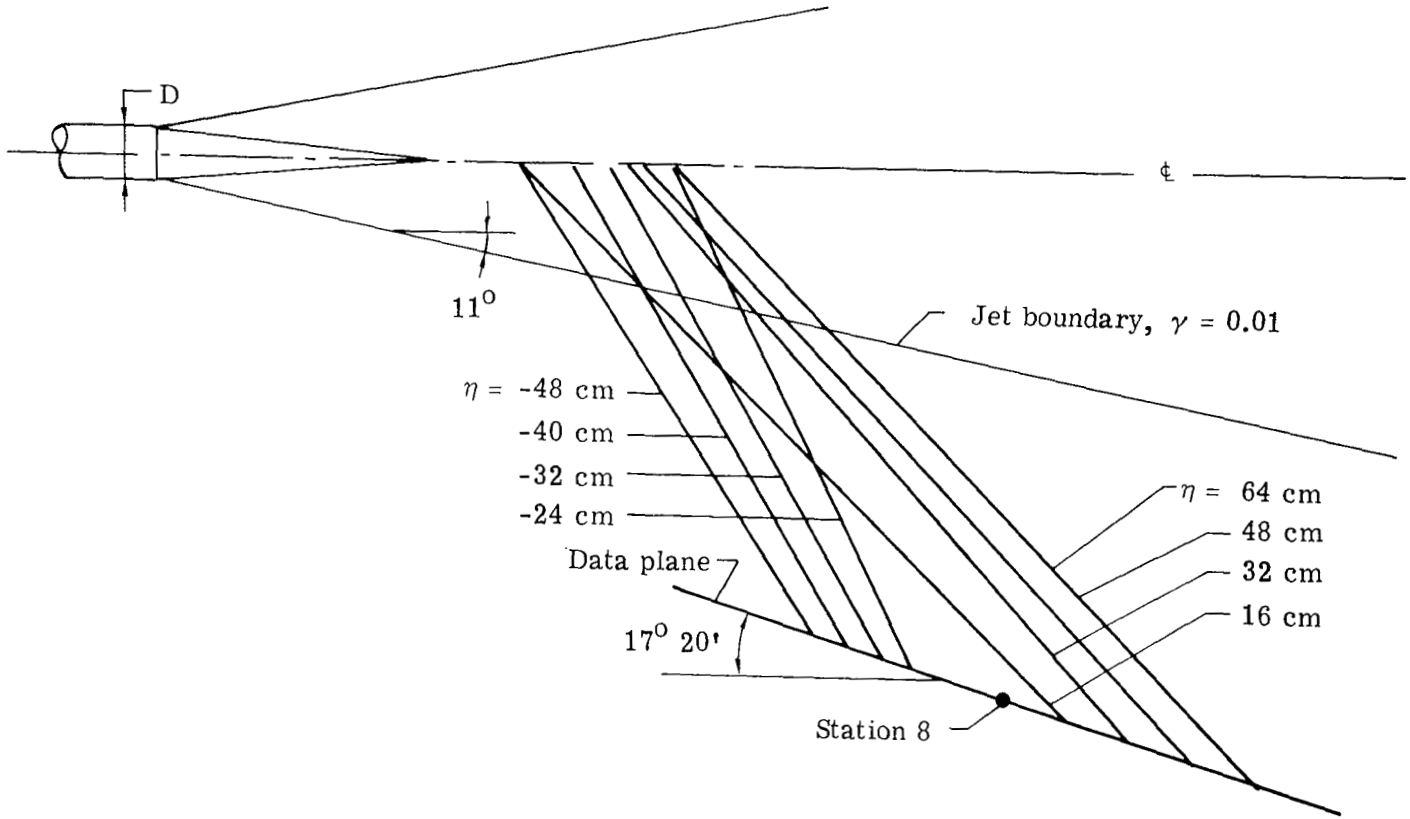

Figure 10.- Ray bundle reconstruction at station 8 as shown on meridian plane of jet.

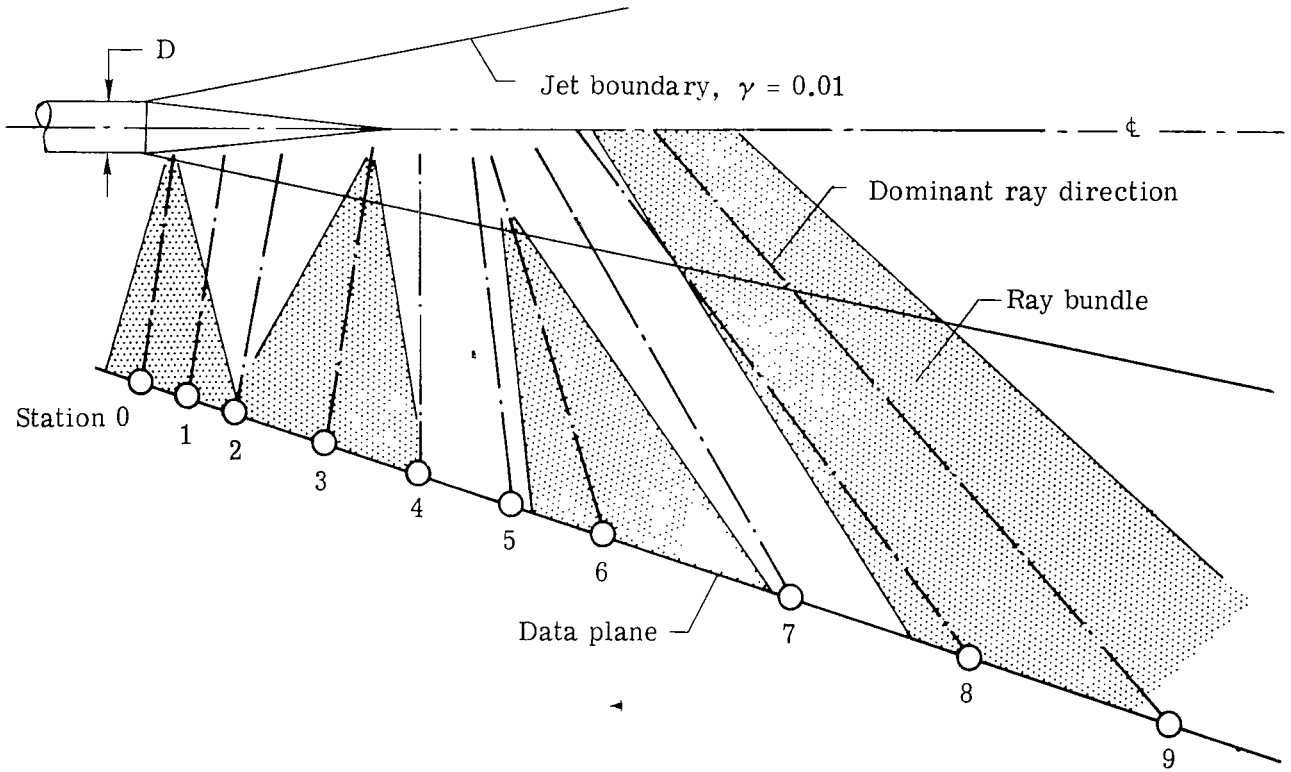

Figure 11.- Average ray direction and ray bundle patterns for stations 0 to 9.

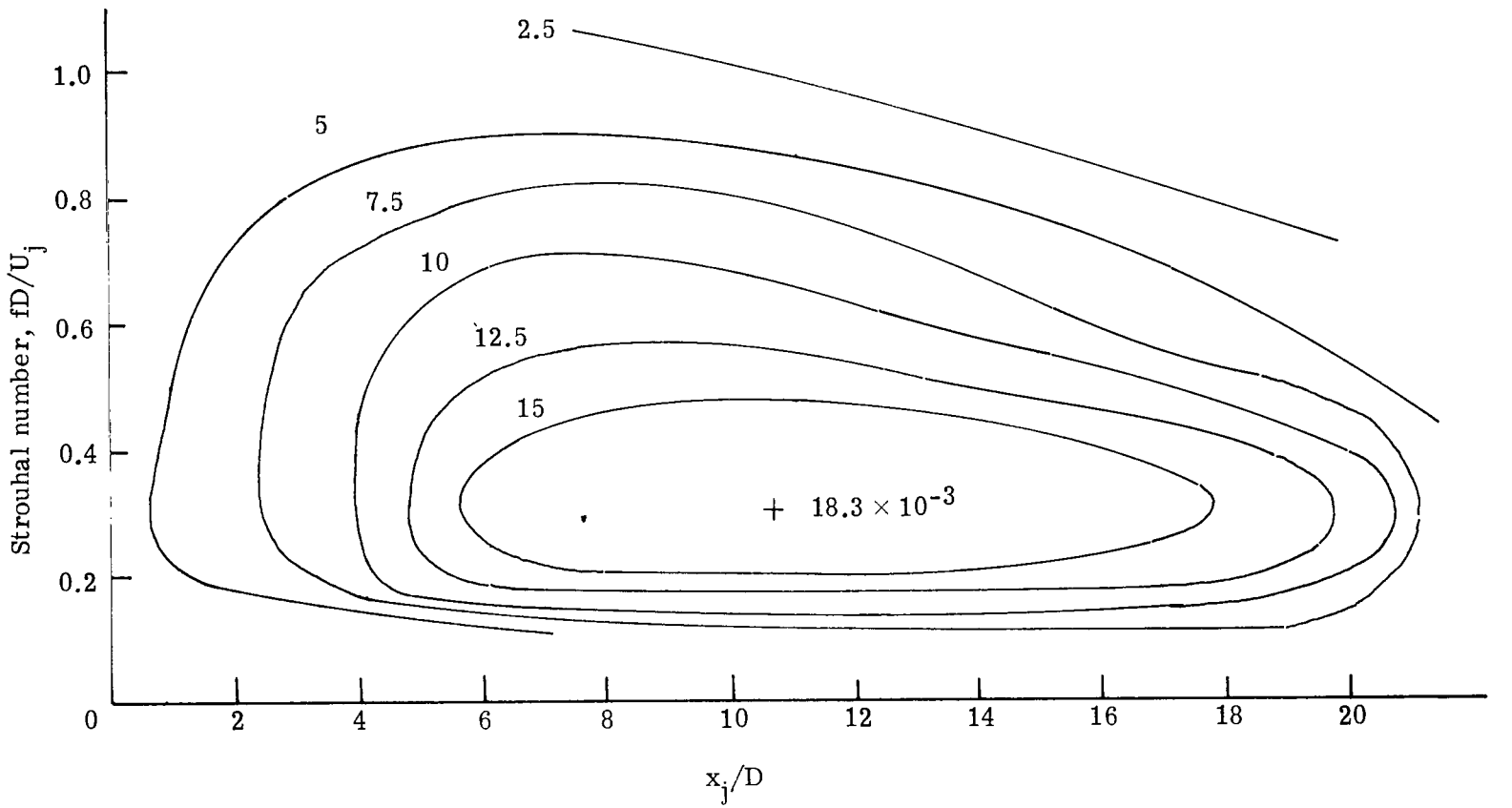

Figure 12.- Contours of constant acoustic power along plane of acoustic measurement, $d\left(W/W_t\right)/dx$. Values of contours are normalized to total sound power of jet.

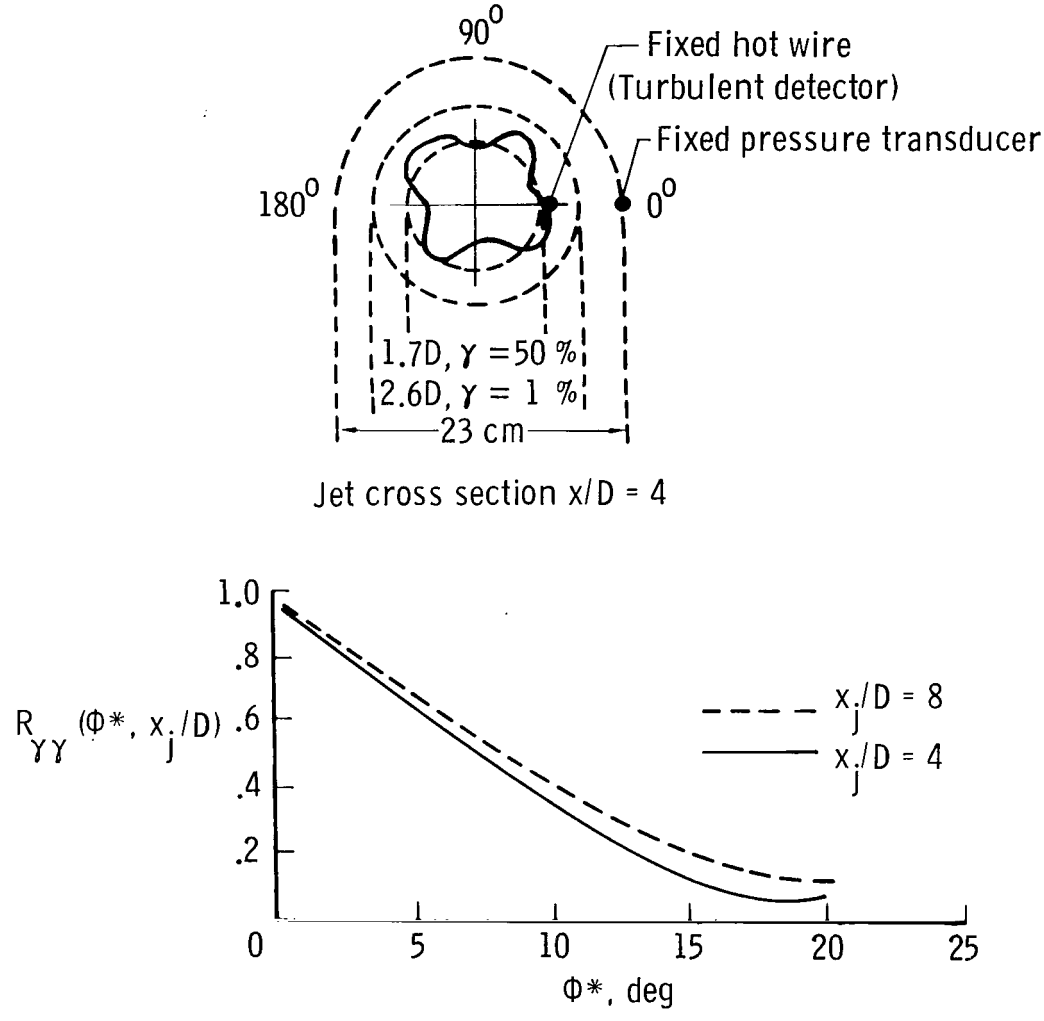

Figure 13.- Measurement of intermittency correlation coefficient around jet.

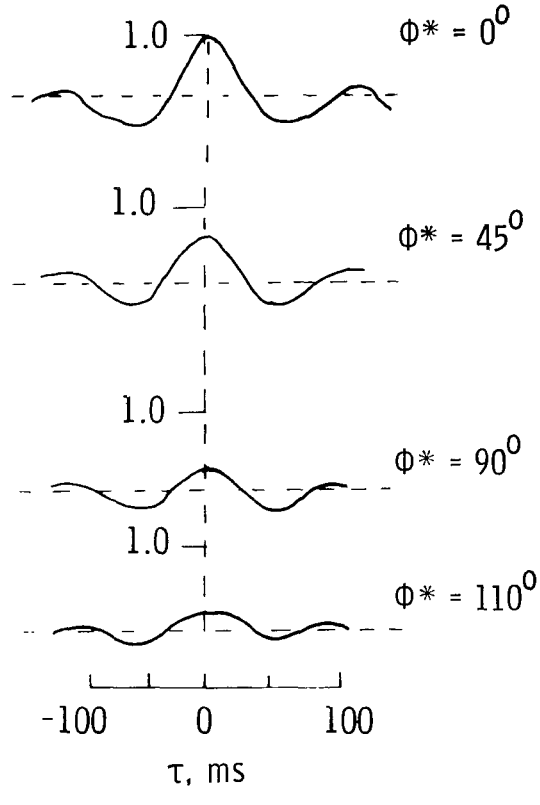

Figure 14.- Measurement of pressure correlation coefficient around jet.

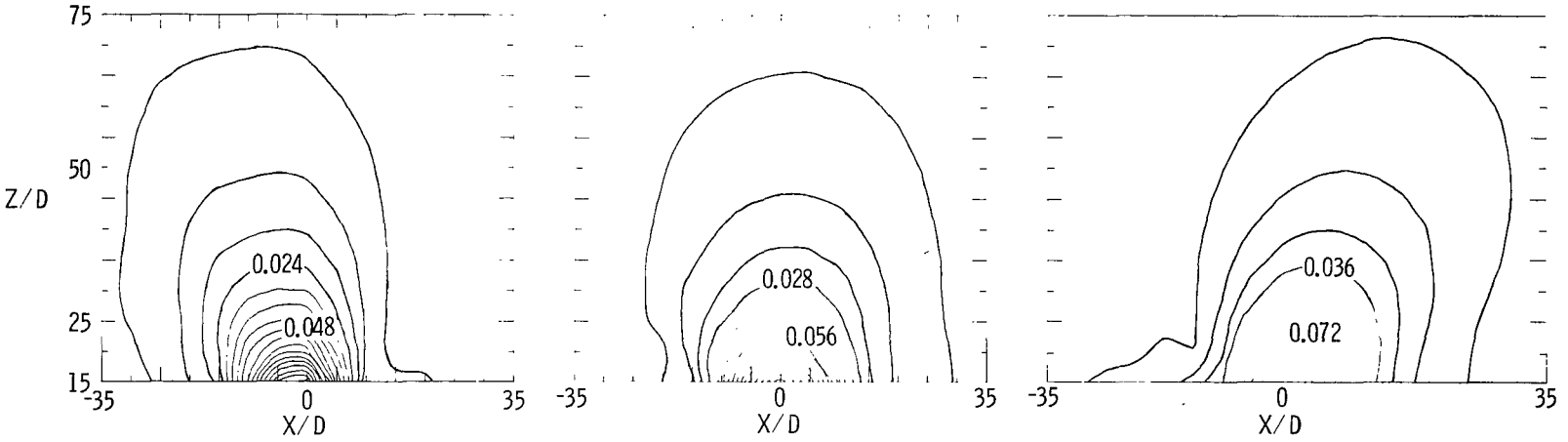

(a) Station 1. (b) Station 3. (c) Station 5.

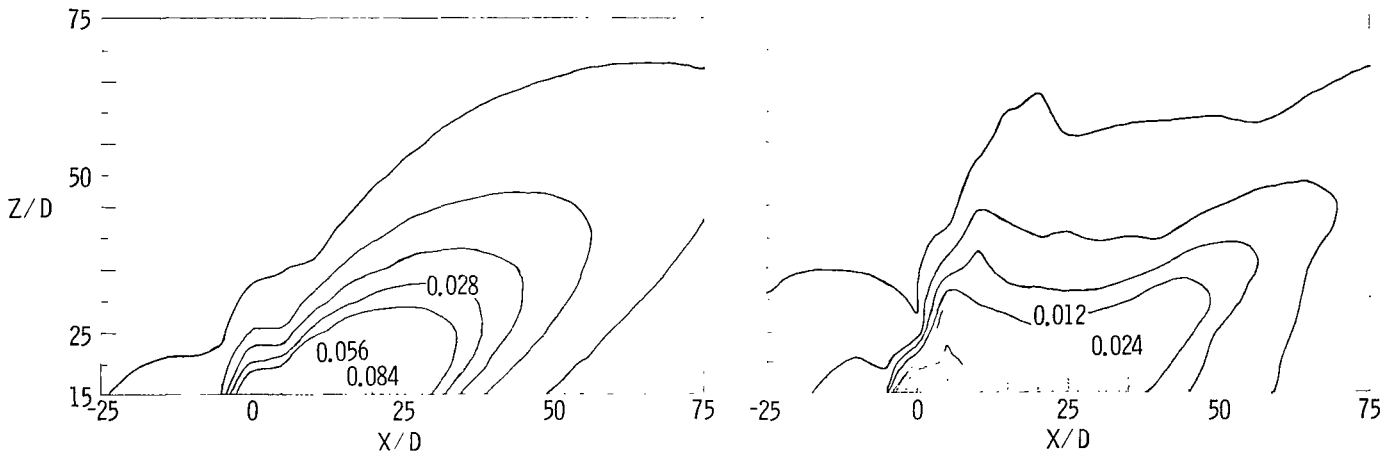

(d) Station 7. (e) Station 9.

Figure 15.- Reconstructed far-field sound-pressure intensity distribution transmission though a unit area at stations 1, 3, 5, 7, and 9. Time shift correction was included. The unit on the contours is 10^{-10} N^2/cm^6.

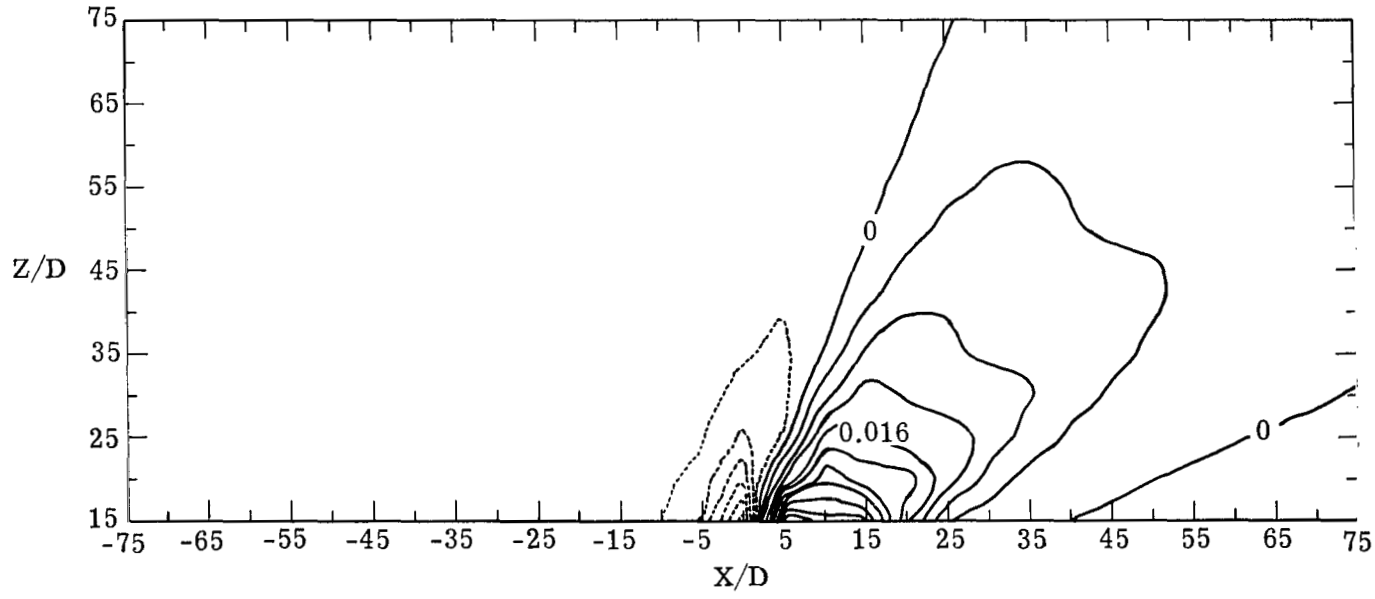

Figure 16.- Reconstructed far-field sound-pressure intensity distribution near station 9 without time shift correction. Units are measured in 10^{-10} N^2/cm^6.

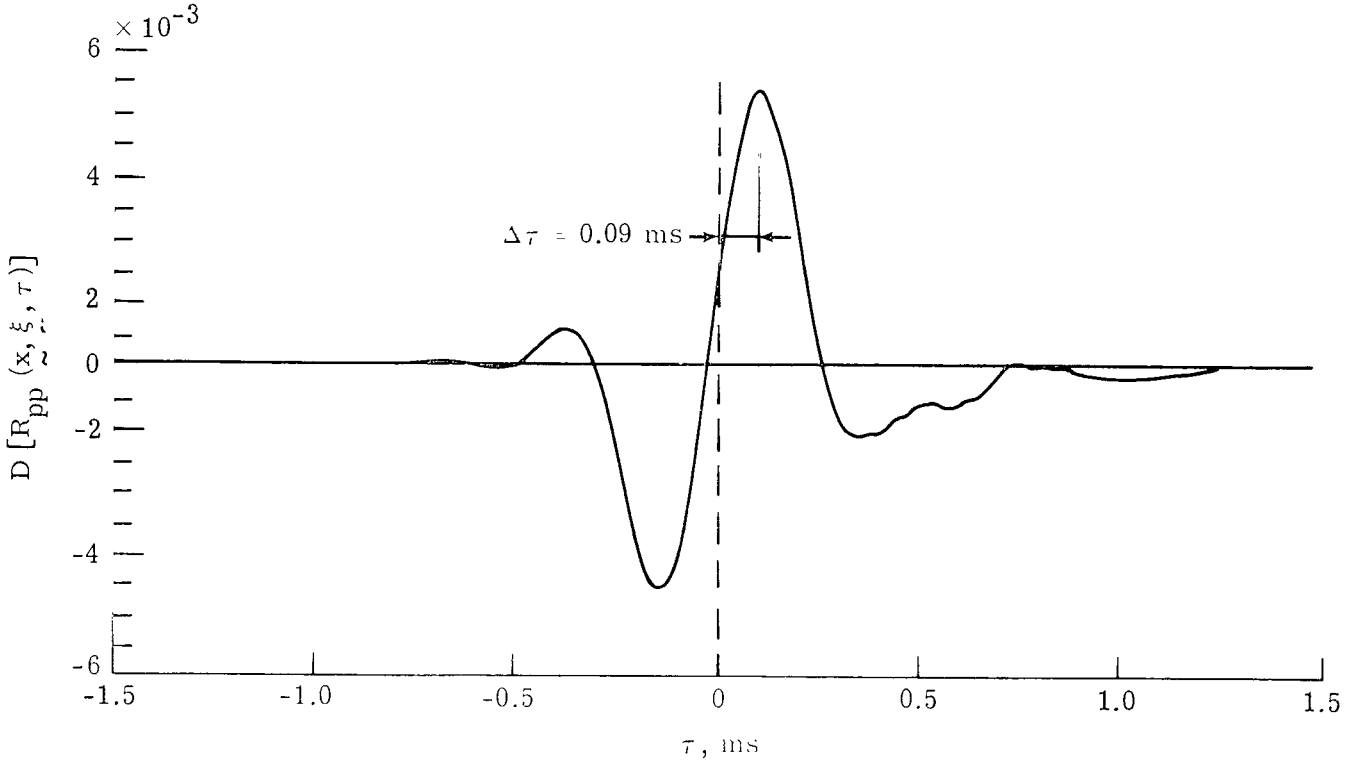

Figure 17.- Typical case of reconstructed correlation function of sound pressure in far field. $D\bar{R}_{pp}(\underset{\sim}{x},\underset{\sim}{\xi},\tau)$ computed at R = 100D. Units are measured in 10^{-10} N^2/cm^6.

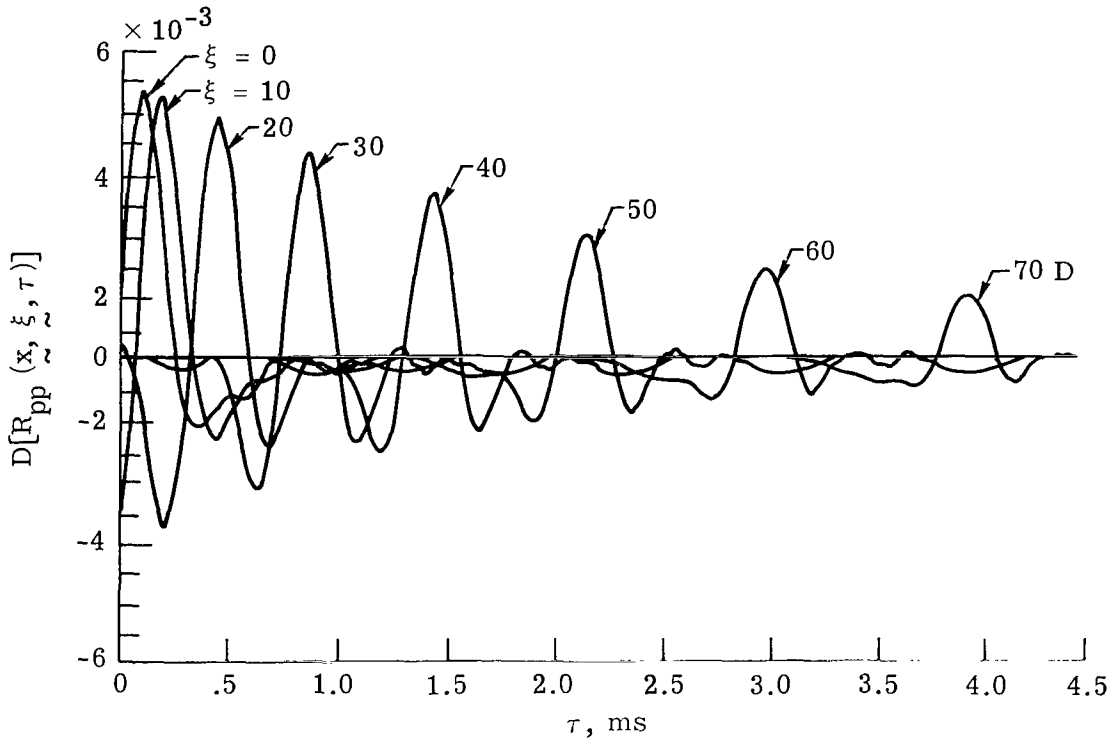

Figure 18.- Typical set of reconstructed sound-pressure correlation function $D\left[R_{pp}(\underset{\sim}{x}, \underset{\sim}{\xi}, \tau)\right]$. Reference point $\underset{\sim}{x}$ was chosen to be a point 100D away from station 5 along a ray 67° from data plane. Units are measured in 10^{-10} N^2/cm^6.

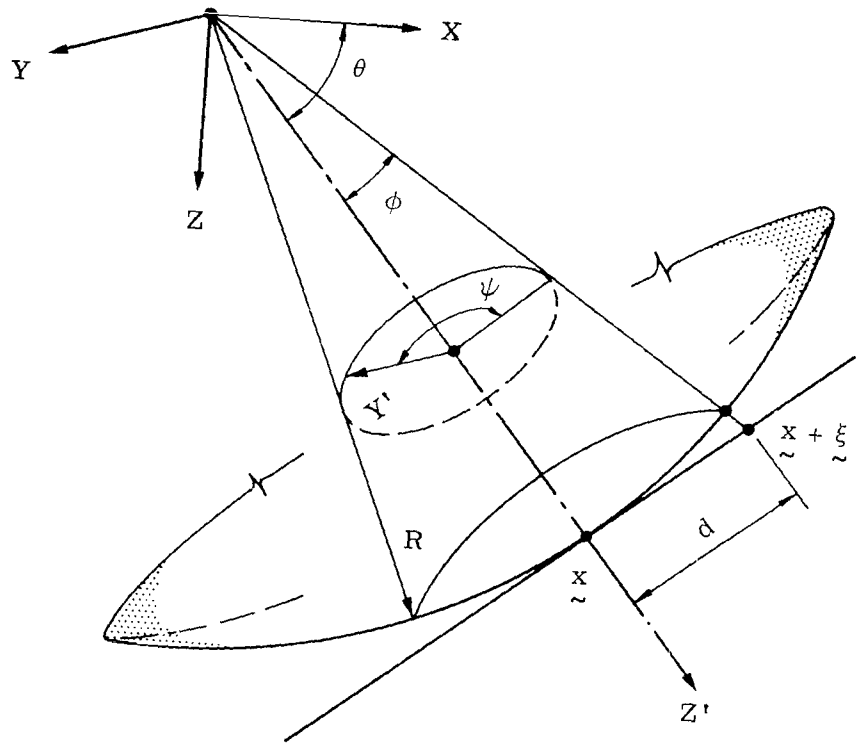

Figure 19.- Local spherical coordinate system related to beam pattern analysis.

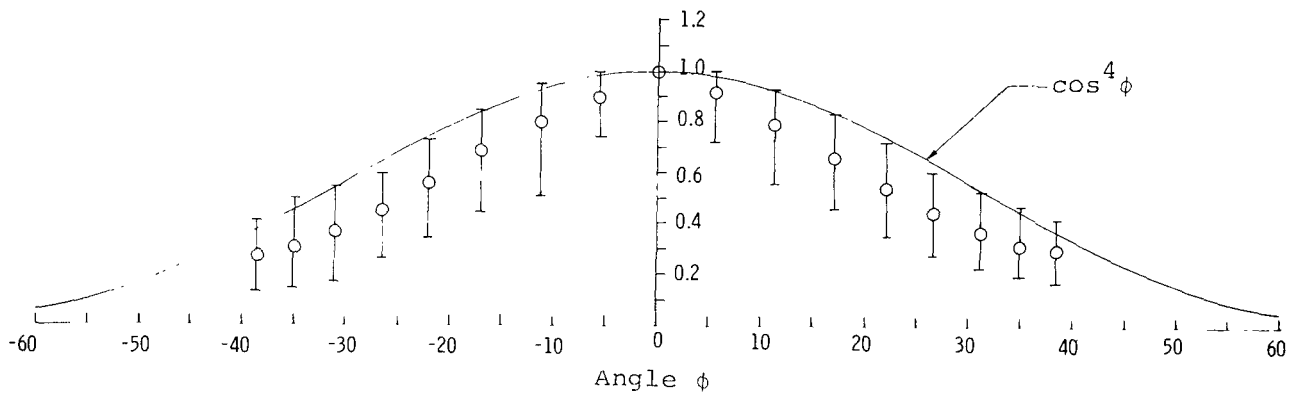

Figure 20.- Values of $\rho_0(\underset{\sim}{x},\phi,\tau_{max})$ across beam pattern.

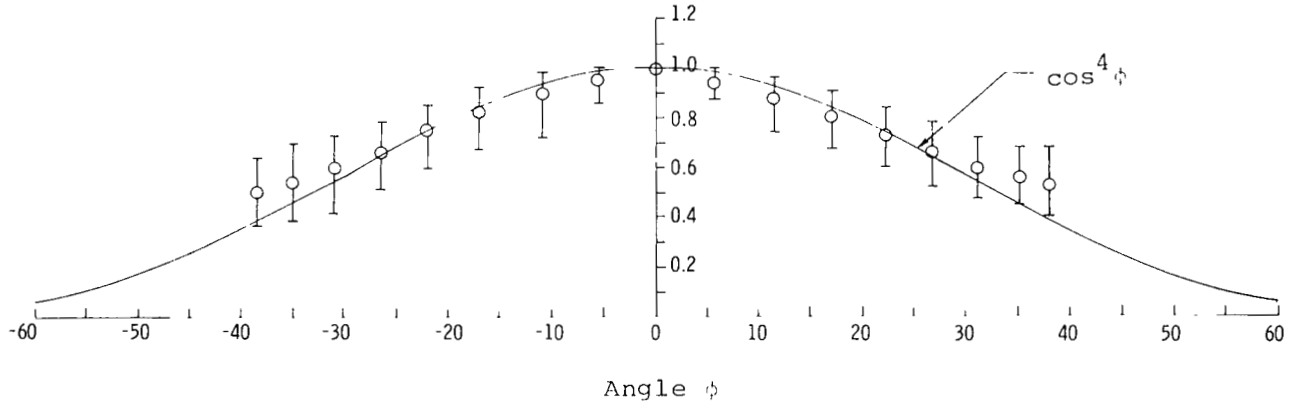

Figure 21.- Values of $\rho_1(\underset{\sim}{x},\phi,\tau_{max})$ across beam pattern.

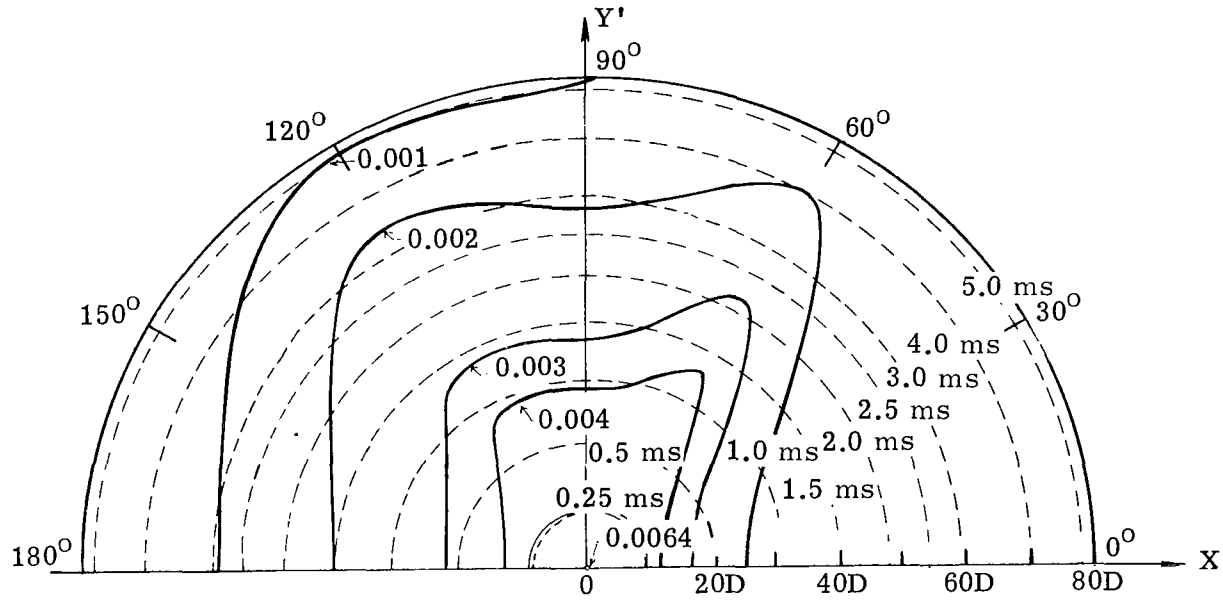

Figure 22.- Contours of amplitude and time of arrival of maximum sound-pressure correlation on plane normal to ray bundle axis. This computation is based on data from station 8. Units are measured in 10^{-10} N^2/cm^6.

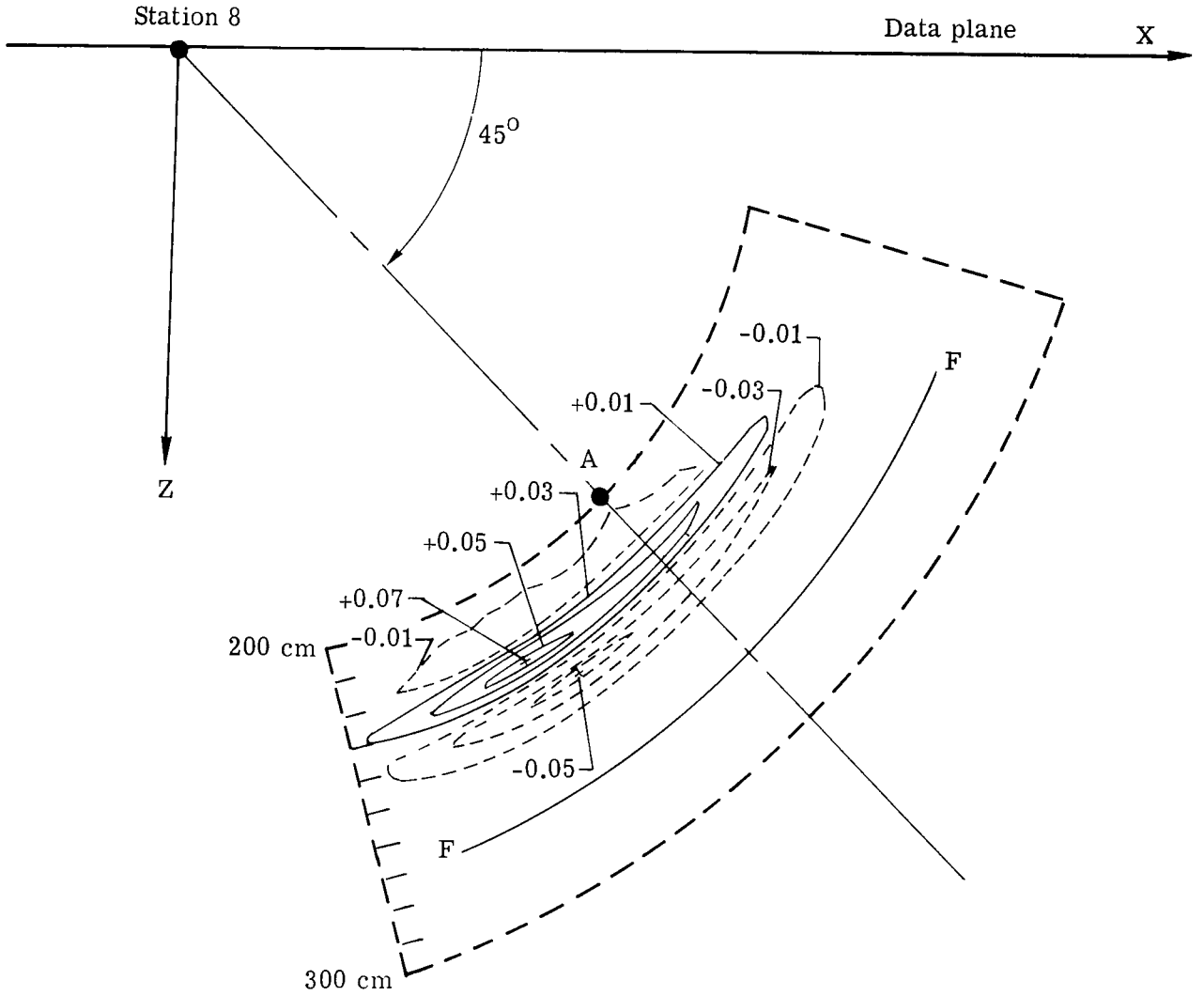

Figure 23.- Correlation contours $D\left[\tilde{R}_{pp}(A, \xi, \tau)\right]$ at fixed delay time $\tau = 1.0$ ms. Units are measured in 10^{-10} N^2/cm^6.

"The aeronautical and space activities of the United States shall be conducted so as to contribute . . . to the expansion of human knowledge of phenomena in the atmosphere and space. The Administration shall provide for the widest practicable and appropriate dissemination of information concerning its activities and the results thereof."

—NATIONAL AERONAUTICS AND SPACE ACT OF 1958

NASA SCIENTIFIC AND TECHNICAL PUBLICATIONS

TECHNICAL REPORTS: Scientific and technical information considered important, complete, and a lasting contribution to existing knowledge.

TECHNICAL NOTES: Information less broad in scope but nevertheless of importance as a contribution to existing knowledge.

TECHNICAL MEMORANDUMS: Information receiving limited distribution because of preliminary data, security classification, or other reasons. Also includes conference proceedings with either limited or unlimited distribution.

CONTRACTOR REPORTS: Scientific and technical information generated under a NASA contract or grant and considered an important contribution to existing knowledge.

TECHNICAL TRANSLATIONS: Information published in a foreign language considered to merit NASA distribution in English.

SPECIAL PUBLICATIONS: Information derived from or of value to NASA activities. Publications include final reports of major projects, monographs, data compilations, handbooks, sourcebooks, and special bibliographies.

TECHNOLOGY UTILIZATION PUBLICATIONS: Information on technology used by NASA that may be of particular interest in commercial and other non-aerospace applications. Publications include Tech Briefs, Technology Utilization Reports and Technology Surveys.

Details on the availability of these publications may be obtained from:

SCIENTIFIC AND TECHNICAL INFORMATION OFFICE

NATIONAL AERONAUTICS AND SPACE ADMINISTRATION

Washington, D.C. 20546